Heavy silicon isotopic composition of silicic acid and biogenic silica in Arctic waters over the Beaufort shelf and the Canada Basin

D. Varela, M. Brzezinski, C. Beucher, J. Jones, K. Giesbrecht, B. Lansard, A. Mucci

▶ **To cite this version:**

D. Varela, M. Brzezinski, C. Beucher, J. Jones, K. Giesbrecht, et al.. Heavy silicon isotopic composition of silicic acid and biogenic silica in Arctic waters over the Beaufort shelf and the Canada Basin. Global Biogeochemical Cycles, 2016, 30 (6), pp.804-824. 10.1002/2015GB005277 . hal-02881295

HAL Id: hal-02881295
https://hal.science/hal-02881295

Submitted on 17 Sep 2020

HAL is a multi-disciplinary open access archive for the deposit and dissemination of scientific research documents, whether they are published or not. The documents may come from teaching and research institutions in France or abroad, or from public or private research centers.

L'archive ouverte pluridisciplinaire **HAL**, est destinée au dépôt et à la diffusion de documents scientifiques de niveau recherche, publiés ou non, émanant des établissements d'enseignement et de recherche français ou étrangers, des laboratoires publics ou privés.

AGU PUBLICATIONS

Global Biogeochemical Cycles

RESEARCH ARTICLE
10.1002/2015GB005277

Key Points:
- Deep Arctic silicic acid isotopic signals are the heaviest of all ocean basins
- Riverine inputs decrease the surface Arctic silicic acid isotopic composition
- Silicon isotopic distribution in the Arctic follows that of major water masses

Supporting Information:
- Supporting Information S1

Correspondence to:
D. E. Varela,
dvarela@uvic.ca

Citation:
Varela, D. E., M. A. Brzezinski, C. P. Beucher, J. L. Jones, K. E. Giesbrecht, B. Lansard, and A. Mucci (2016), Heavy silicon isotopic composition of silicic acid and biogenic silica in Arctic waters over the Beaufort shelf and the Canada Basin, *Global Biogeochem. Cycles, 30*, 804–824, doi:10.1002/2015GB005277.

Received 20 SEP 2015
Accepted 28 APR 2016
Accepted article online 30 APR 2016
Published online 4 JUN 2016

©2016. American Geophysical Union. All Rights Reserved.

Heavy silicon isotopic composition of silicic acid and biogenic silica in Arctic waters over the Beaufort shelf and the Canada Basin

D. E. Varela[1,2], M. A. Brzezinski[3,4], C. P. Beucher[2,3], J. L. Jones[3], K. E. Giesbrecht[2], B. Lansard[5,6], and A. Mucci[5]

[1]Department of Biology, University of Victoria, Victoria, British Columbia, Canada, [2]School of Earth and Ocean Sciences, University of Victoria, Victoria, British Columbia, Canada, [3]Marine Science Institute, University of California, Santa Barbara, California, USA, [4]Department of Ecology Evolution and Marine Biology, University of California, Santa Barbara, California, USA, [5]GEOTOP and Department of Earth and Planetary Sciences, McGill University, Montréal, Quebec, Canada, [6]Laboratoire des Sciences du Climat et de l'Environnement, LSCE/IPSL, CEA-CNRS-UVSQ, Université Paris-Saclay, Gif-sur-Yvette, France

Abstract The silicon isotopic composition of silicic acid ($\delta^{30}Si(OH)_4$) and biogenic silica ($\delta^{30}Si\text{-}bSiO_2$) were measured for the first time in marine Arctic waters from the Mackenzie River delta to the deep Canada Basin in the late summer of 2009. In the upper 100 m of the water column, $\delta^{30}Si(OH)_4$ signals (+1.82‰ to +3.08‰) were negatively correlated with the relative contribution of Mackenzie River water. The biogenic Si isotope fractionation factor estimated using an open system model, $^{30}\varepsilon = -0.97 \pm 0.17$‰, agrees well with laboratory and global-ocean estimates. Nevertheless, the $\delta^{30}Si$ dynamics of this region may be better represented by closed system isotope models that yield lower values of $^{30}\varepsilon$, between −0.33‰ and −0.41‰, depending on how the contribution of sea-ice diatoms is incorporated. In the upper 400 m, $\delta^{30}Si\text{-}bSiO_2$ values were among the heaviest ever measured in marine suspended $bSiO_2$ (+2.03‰ to +3.51‰). A positive correlation between $\delta^{30}Si\text{-}bSiO_2$ and sea-ice cover implies that heavy signals can result from isotopically heavy sea-ice diatoms introduced to pelagic assemblages. Below the surface $bSiO_2$ production zone, the $\delta^{30}Si(OH)_4$ distribution followed that of major water masses. Vertical $\delta^{30}Si(OH)_4$ profiles showed a minimum (average of +1.84 ± 0.10‰) in the upper halocline (125–200 m) composed of modified Pacific water and heavier average values (+2.04 ± 0.11‰) in Atlantic water (300–500 m deep). In the Canada Basin Deep Water (below 2000 m), $\delta^{30}Si(OH)_4$ averaged +1.88 ± 0.12‰, which represents the most positive value ever measured anywhere in the deep ocean. Since most $Si(OH)_4$ enters the Arctic from shallow depths in the Atlantic Ocean, heavy deep Arctic $\delta^{30}Si(OH)_4$ signals likely reflect the influx of relatively heavy intermediate Atlantic waters. A box model simulation of the global marine $\delta^{30}Si(OH)_4$ distribution successfully reproduced the observed patterns, with the $\delta^{30}Si(OH)_4$ of the simulated deep Arctic Ocean being the heaviest of all deep-ocean basins.

1. Introduction

Diatoms, the dominant siliceous microplankton in marine waters, contribute ~20% of the annual carbon (C) fixed by primary producers on Earth [*Field et al.,* 1998] and ~40% of annual marine C fixation [*Nelson et al.,* 1995]. Diatoms can therefore play a critical role in the marine biological C pump and consequently in Earth's climate. These unicellular algae require silicon (Si) to form their opaline silica cell walls, and as the largest consumers of dissolved Si in marine surface waters, they also control the cycling of Si. During the physiological uptake of Si, diatoms discriminate against the heavy Si isotopes [*De La Rocha et al.*, 1997] resulting in systematic variations in the natural Si isotopic composition ($\delta^{30}Si$) of biogenic silica ($bSiO_2$) and of dissolved Si (silicic acid; $Si(OH)_4$) in ocean basins. Therefore, the Si isotopic composition of both $Si(OH)_4$ ($\delta^{30}Si(OH)_4$) and of $bSiO_2$ ($\delta^{30}Si\text{-}bSiO_2$) can potentially be used as proxies of marine Si dynamics and diatom production over broad spatial and long temporal scales [e.g., *Pichevin et al.*, 2009; *Cardinal et al.*, 2007; *Beucher et al.*, 2011; *Fripiat et al.*, 2011a; *Brzezinski and Jones*, 2015]. In the modern ocean, natural variations in seawater $\delta^{30}Si$ have been used to quantify annual $Si(OH)_4$ uptake in surface waters [e.g., *Varela et al.,* 2004; *Fripiat et al.*, 2011b], to determine vertical nutrient supply rates [e.g., *Fripiat et al.,* 2011a, 2011b], and to identify water masses [e.g., *Reynolds et al.*, 2006; *Brzezinski and Jones*, 2015], whereas variations in $\delta^{30}Si$ signals of sedimentary diatomaceous opal have been used to reconstruct nutrient utilization histories over geological time scales [e.g., *De La Rocha et al.,* 1998; *Beucher et al.*, 2007;

Horn et al., 2011]. Further insights into the marine Si cycle can also be obtained from the δ^{30}Si composition of deep sea sponge spicules, which have proven useful for reconstructions of paleo-$Si(OH)_4$ concentrations of deep marine waters [*Ellwood et al.*, 2010; *Hendry et al.*, 2010; *Wille et al.*, 2010].

Application of δ^{30}Si as a proxy for Si utilization by diatoms in surface waters requires an understanding of the extent to which Si isotope fractionation, the biological pump, and ocean circulation contribute to the redistribution of Si isotopes within the modern ocean. Of particular interest is the variation in $\delta^{30}Si(OH)_4$ signals and $Si(OH)_4$ concentrations in ventilating water masses that supply $Si(OH)_4$ to surface waters, as these parameters are both required to estimate the Si isotope fractionation factor, $^{30}\varepsilon$, from field data [*Varela et al.,* 2004; *Reynolds et al.,* 2006; *Beucher et al.,* 2008] and to interpret $\delta^{30}Si\text{-}bSiO_2$ paleorecords [*Beucher et al.,* 2007; *Hendry and Brzezinski,* 2014]. Progress on this front is currently hindered by the limited global data set of $\delta^{30}Si(OH)_4$ and $\delta^{30}Si\text{-}bSiO_2$ measurements, and therefore, temporal and spatial variations in $\delta^{30}Si(OH)_4$ in ventilating water masses are poorly understood. Deeper in the water column, $\delta^{30}Si(OH)_4$ signals show notable differences among deep-ocean basins, with values declining along the flow path of the meridional overturning circulation (MOC) [*Reynolds,* 2009]. The measured 0.3‰ decrease in $\delta^{30}Si(OH)_4$ between the deep Atlantic Ocean and the Pacific Ocean has been reproduced in box models that couple the MOC with the Si cycle [*Reynolds,* 2009], and more complex global circulation models [*de Souza et al.*, 2014; *Holzer and Brzezinski*, 2015] provide further evidence for a strong linkage between the MOC and Si isotope distribution in deep waters. Nevertheless, missing from these models is an evaluation of the role of the Arctic Ocean due in part to the complete lack of δ^{30}Si data for Arctic marine waters.

Here, we extend the analysis of the oceanic distribution of $[Si(OH)_4]$, $[bSiO_2]$, $\delta^{30}Si(OH)_4$, and $\delta^{30}Si\text{-}bSiO_2$ to the Arctic Ocean, the smallest and shallowest of the world's oceans [*Eakins and Sharman,* 2010]. The Arctic Ocean is connected to, and influenced by, both the Pacific and the Atlantic Oceans. Fresh water input into the Arctic Ocean is large relative to its size, with inputs dominated by the Mackenzie River in Canada and the Ob, Yenisey and Lena Rivers in Siberia [*McClelland et al.*, 2012] (Figure 1a). The circulation of the Arctic Ocean is influenced by the combined inflow of relatively warm, saline Atlantic water and cool, less saline Pacific water. The North Atlantic Current dominates the inflow to the Arctic Ocean, forming the core of the Arctic thermohaline circulation. As these relatively warm, dense waters circulate through the Arctic Ocean, they either cool, becoming denser to form the deep arm of the Arctic thermohaline circulation, or mix with river, sea-ice melt, and/or the less saline waters of the Pacific Ocean to form the shallow arm of this density-driven flow [*Carmack and Wassmann,* 2006]. Arctic deep waters (>2000 m) are relatively isolated from other ocean basins due to the shallow sills that restrict exchange with both the Atlantic and Pacific Basins. Exchange within the deep Arctic Ocean is also restricted by the Alpha, Lomonosov and Mendeleev Ridges, which rise from the ocean floor to 400 to 1500 m below sea level to define the boundaries of the Canada, Makarov, and Eurasian basins (Figure 1a).

Marine primary production in the Arctic varies considerably among regions, with the offshore waters of the central basins being the least productive [e.g., *Gosselin et al.*, 1997; *Carmack et al.*, 2004; *Tremblay et al.,* 2012; *Varela et al.,* 2013]. *Varela et al.* [2013] documented the lowest levels of pelagic primary and new production in the South Beaufort Sea and Canada Basin (BS-CB) during the summers of 2007–2008, when compared to other Arctic and Subarctic domains around northern North America, from the NE Pacific to the NW Atlantic. Specifically, along the same shelf-basin transect reported in the present study, phytoplankton production in the surface mixed layer decreased by an order of magnitude, from 2.2 mg C m^{-3} d^{-1} (station S1; Figure 1b) on the Beaufort Shelf (BS) to 0.2–0.5 mg C m^{-3} d^{-1} (stations L1 and L2, respectively) in the offshore waters of the Canada Basin (CB) in late summer of 2009 [*Brown et al.,* 2014]. Low diatom productivity in the BS-CB domain resulted in the lowest amounts of suspended biogenic particles (C, N, and Si) in the euphotic zone of the same region, in comparison to other Subarctic and Arctic domains in northern North America [*Wyatt et al.,* 2013]. Dissolved nutrient concentrations, including $Si(OH)_4$, in the upper ocean decreased markedly from the NE Pacific through the Arctic waters north of North America to the NW Atlantic, with intermediate values (average $[Si(OH)_4]$ of about 5 μmol L^{-1} at 2–10 m depth) in the BS-CB domain [*Varela et al.*, 2013]. It is presently unknown how the observed variability in $bSiO_2$ production and $Si(OH)_4$ utilization translates into variability in δ^{30}Si signals along a shelf-basin transition in the Arctic Ocean.

The present study was part of the 2007–2008 International Polar Year (IPY) and the Canadian contribution to the International GEOTRACES program and took place during the late summer of 2009 in the Beaufort Sea

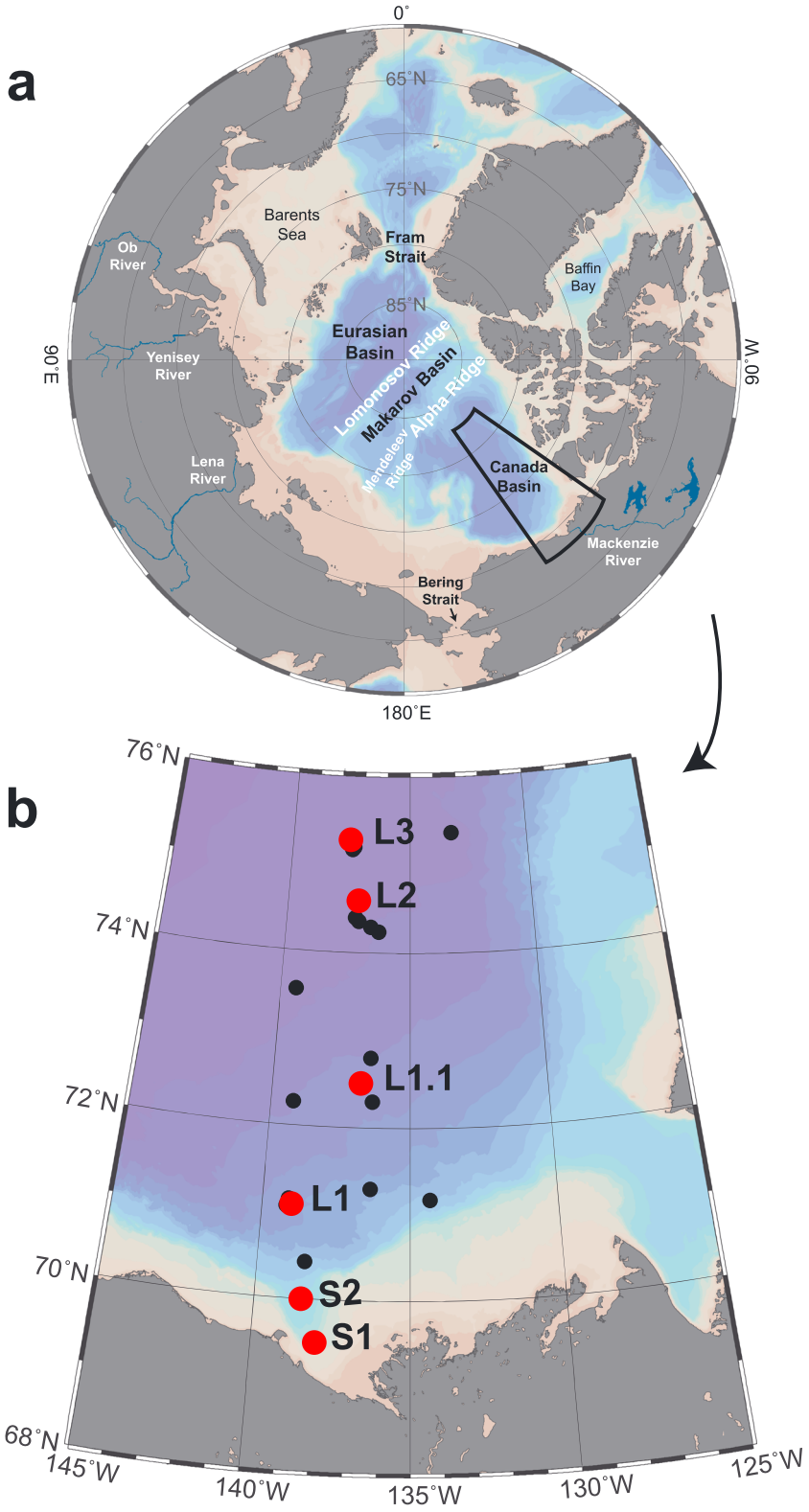

Figure 1. (a) Map of the Arctic Ocean indicating the geographic features of interest in this study. (b) Location of the six stations (red circles) sampled from the Beaufort Sea continental shelf to the deep Canada Basin for the measurement of Si isotopes and dissolved and particulate Si concentrations during the Canadian IPY-GEOTRACES expedition in August–September 2009. Black circles indicate the location of the underway stations sampled for Si isotopic measurements.

along a transect from the continental shelf near the outflow of the Mackenzie River to the open waters of the Canada Basin. Here, we present the first water column δ^{30}Si measurements of the Arctic Ocean, both in the dissolved and particulate Si pools.

2. Material and Methods

2.1. Sampling

The Canadian IPY-GEOTRACES sampling program was carried out from 27 August 2009 to 12 September 2009 as part of Leg 3a of the 2009 CCGS Amundsen Expedition (ArcticNet 0903) in the Arctic Ocean.

Water samples for the measurement of $\delta^{30}Si(OH)_4$ as well as the concentrations of $Si(OH)_4$, $bSiO_2$ and lithogenic silica ($lSiO_2$) were collected throughout the water column using a SeaBird 911 conductivity-temperature-depth (CTD) sensor and a rosette package equipped with 24 12-L Niskin bottles at six stations distributed from the Mackenzie River delta on the Beaufort Sea continental shelf to the deep Canada Basin (Figure 1b). Bottom depths ranged from 58 m at station S1 near the Mackenzie River delta to 3485 m at station L3 in the Canada Basin. Additional surface water samples for the same measurements were obtained from ~7 m depth with the underway continuous pumping system at selected locations along the ship's cruise track (Figure 1b).

Samples (2–4 L) for $\delta^{30}Si(OH)_4$ determination were filtered either through 0.8/0.2 μm Acropak™ 500 Supor® membrane filter cartridges or through 0.6 μm polycarbonate membrane filters, and the filtrate stored in acid-washed polypropylene bottles at room temperature in the dark. Samples for $Si(OH)_4$ concentration were filtered through 0.6 μm polycarbonate filters into polypropylene containers and kept cold until measured onboard ship. Suspended particulate matter for $bSiO_2$ and $lSiO_2$ concentrations was collected on 0.6 μm polycarbonate filters, dried at 60°C, and stored at room temperature prior to analysis onshore.

Suspended particulate matter for $\delta^{30}Si\text{-}bSiO_2$ determination was collected throughout the water column using large-volume in situ pumps (McLane®) at three stations (L1, L1.1, and L2) and from ~7 m depth with the underway continuous pumping system at additional selected locations along the ship's cruise track (Figure 1b). For each sample, 100 to 300 L of seawater were filtered through 142 mm 0.8 μm Supor® or 0.6 μm polycarbonate filters. Filters were dried at 60°C and stored at room temperature prior to δ^{30}Si analysis on shore.

Sea ice concentration data for the study period were retrieved in October 2013 from the Integrated Climate Date Center (http://icdc.zmaw.de/) at the University of Hamburg (Hamburg, Germany), where sea ice concentrations were calculated by applying the ARTIST sea-ice (ASI) algorithm to brightness temperatures from the Advanced Microwave Scanning Radiometer on board the EOS (AMSR-E) satellite. A five-day mean of these sea-ice concentrations (from 5 days prior to sampling up to the sampling date) was calculated to account for short-term changes in the amount of sea ice and potential supply of sea-ice diatoms to the surface waters during ice melting.

2.2. Analytical Methods

Silicic acid concentrations were determined at sea using a Bran and Luebbe AutoAnalyzer II according to the method described by *Whitledge et al.* [1981]. Biogenic SiO_2 concentrations were measured using the sodium hydroxide digestion method described in *Brzezinski and Nelson* [1989]. Lithogenic SiO_2 concentrations were determined on a subset of samples using a sequential sodium hydroxide-hydrofluoric acid digestion [*Brzezinski and Nelson*, 1989].

Preparation of seawater for Si isotope analysis was performed after samples were returned to the onshore laboratory. Samples for $\delta^{30}Si(OH)_4$ measurements were processed as described in *Beucher et al.* [2008]. Briefly, $Si(OH)_4$ was extracted from seawater by precipitation (24 h) as triethylamine silicomolybdate, which was then combusted to form crystobalite, SiO_2 [*De La Rocha et al.*, 1996]. Samples containing $< 6\ \mu mol\ L^{-1}$ of $Si(OH)_4$ were prepared using one of two recovery methods. The first method employed magnesium-induced coprecipitation (modified MAGIC method of *Karl and Tien* [1992]) to scavenge the $Si(OH)_4$ from the sample, as described by *Brzezinski et al.* [2003]. Magnesium hydroxide ($Mg(OH)_2$) was precipitated from seawater by the addition of aqueous sodium hydroxide (with low Si, Fluka brand #71692) to a final concentration of 0.05 *M*. The resulting precipitate and scavenged Si were left to settle for at least 24 h before recovery by

centrifugation. The precipitate was dissolved using a very small volume of 5 *M* ACS reagent grade hydrochloric acid, and the resulting $Si(OH)_4$ was converted to SiO_2 by precipitation as triethylamine silicomolybdate followed by combustion as described above. The second method simply involved allowing the precipitation of $Si(OH)_4$ as triethylamine silicomolybdate to proceed for 7 days for samples with low $Si(OH)_4$ concentration, instead of the 1-day precipitation used for samples containing $> 6\ \mu mol\ L^{-1}$ of $Si(OH)_4$. This method was based on previous findings by *De La Rocha et al.* [1996], who documented a recovery of 99.3 ± 0.1% for a 7-day precipitation.

Biogenic SiO_2 for δ^{30}Si-$bSiO_2$ analysis was dissolved in a 95°C aqueous sodium carbonate solution following the method of *DeMaster* [1981] and converted to SiO_2 as described above for $\delta^{30}Si(OH)_4$. Sodium carbonate was used for the digestion rather than sodium hydroxide to minimize the dissolution of $lSiO_2$.

The SiO_2 derived from both $Si(OH)_4$ and $bSiO_2$ was converted to cesium hexafluosilicate and decomposed with sulfuric acid in a modified Kiel III inlet system to generate SiF_4 gas, which was analyzed for Si isotopic composition on a Finnigan MAT 252 isotope ratio mass spectrometer [*Brzezinski et al.,* 2006]. Isotope values are expressed relative to the NBS28 quartz sand reference material using the delta notation (‰):

$$\delta^{30}Si = \left(\frac{\left({}^{30}Si/{}^{28}Si\right)_{sample}}{\left({}^{30}Si/{}^{28}Si\right)_{NBS28}} - 1 \right) \times 1000 \quad (1)$$

Each isotope value presented in this study is the mean (±1 standard deviation, SD) of duplicate or triplicate measurements of the same field sample. The in-house secondary standard "Big Batch" was run in the mass spectrometer every 8–12 field samples. During this study, the Big Batch δ^{30}Si measurements yielded an average (±SD) δ^{30}Si value of −10.40‰ ± 0.18‰ for $n = 118$, compared to the consensus value of −10.48‰ ± 0.27‰ [*Reynolds et al.,* 2007].

Bias in δ^{30}Si-$bSiO_2$ measurements due to contamination from partial dissolution of $lSiO_2$ during the digestion of $bSiO_2$ was evaluated in a representative number of samples throughout the water column. The $lSiO_2$ remaining after the sodium carbonate digestion was rinsed, dissolved in HF, precipitated with acid-molybdate/triethylamine, converted to cesium hexafluosilicate, and its isotopic composition determined. The resulting average δ^{30}Si-$lSiO_2$ value of −0.03 ± 0.12‰ ($n = 4$) together with the $bSiO_2$ and $lSiO_2$ content of the samples were used to estimate this potential bias as follows. The mass of $lSiO_2$ dissolving during the sodium carbonate digestion was estimated from the change in $Si(OH)_4$ concentration during the time-course digestions of the particulate Si samples. The increase in $Si(OH)_4$ concentration over the first 40 min of the digestion reflected the solubilization of $bSiO_2$, but no further increase in $Si(OH)_4$ was detectable between 40 min (the shortest time interval tested) and 120 min. Assuming that only $lSiO_2$ dissolved between 40 and 120 min, these results indicate that very little or no $lSiO_2$ was solubilized by this procedure. In fact, given our analytical detection limit for $Si(OH)_4$ in these experiments, 1–3% of the $lSiO_2$ present in the samples could have dissolved without causing a detectable signal in $Si(OH)_4$ concentrations. Although *Ragueneau and Tréguer* [1994] indicate that up to 15% of $lSiO_2$ can dissolve during the sodium hydroxide digestion, our own measurements provide evidence that $lSiO_2$ dissolution in our samples is much lower (1–3%). Assuming that the measured δ^{30}Si-$bSiO_2$ in a sample represents the average δ^{30}Si values of $bSiO_2$ and $lSiO_2$ weighted by their respective masses ([$bSiO_2$] measured and [$lSiO_2$] assumed as 1–3% of measured total [$lSiO_2$]), the reported δ^{30}Si-$bSiO_2$ values may be underestimated by 0.1–0.3‰.

3. Results

3.1. Physical Properties

Temperature and salinity distributions along the sampling transect revealed four main layers in the physical structure of the water column: a low-salinity surface layer overlying a strong, cold, halocline; a warm intermediate layer; and a cold, more saline, deep layer (Figure 2a). The low-salinity surface layer (0–100 m) showed variable temperatures (−1.4 to +3.0°C) and was influenced by both sea-ice melt and the warm, fresh surface water associated with the outflow of the Mackenzie River, though the riverine influence was confined mainly to the two stations (S1 and S2) at the southern end of the section. Surface salinity increased with distance offshore from the continental shelf and then decreased again north of 72°N latitude (Figure 2a). Meridional gradients in temperature and salinity were generally weak at deeper depths except at station L1 near 71°N, where strong salinity variations were observed within the halocline. The TS data from the vertical

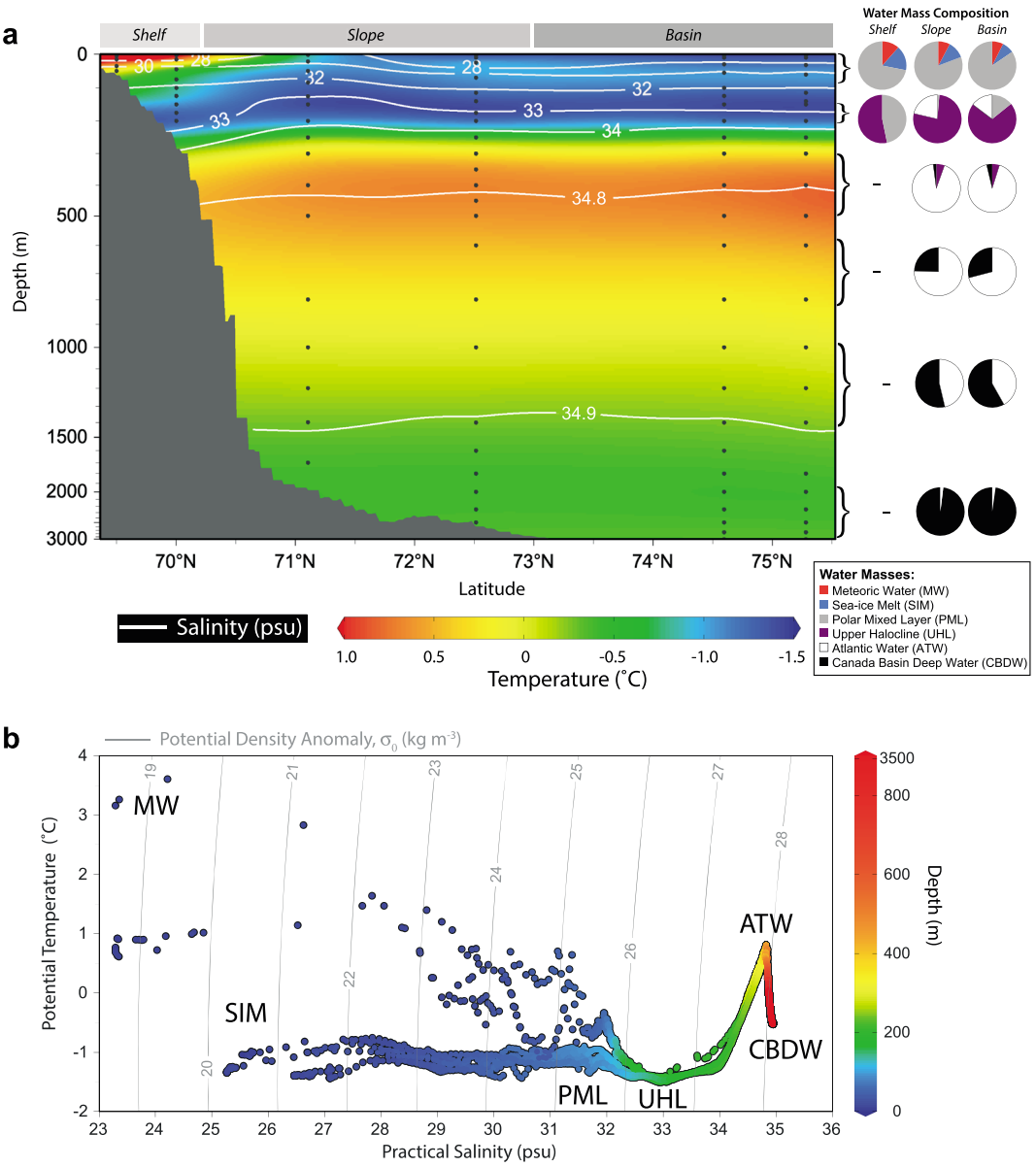

Figure 2. (a) Vertical and latitudinal distribution of temperature (color contours) and salinity (contour lines) for the six stations along the study section. Pie charts represent the water mass composition for the shelf, slope, and basin waters over the depth ranges indicated by the brackets (see supporting information). Shelf, slope, and basin waters are indicated by the grey bars along the top of Figure 2a. Black dots indicate the sampling depths. (b) Potential temperature (°C) versus practical salinity diagram for all six stations. For Figure 2b, data from full CTD profiles were used. Color of symbols indicates depth. Grey contour lines denote lines of constant potential density anomalies ($\sigma_\emptyset = \rho_\emptyset - 1000$, kg m^{-3}; $\rho_\emptyset$ = constant potential density).

profiles of the six stations (Figure 2b) were variable at low salinities and then converged at a salinity of ~33.1 and a temperature of −1.4°C, corresponding to the Pacific-origin waters that form the upper halocline between ~150 and 200 m. The observed temperature maximum at +0.8°C and salinity ~34.8 correspond to Atlantic-origin waters, between 300 and 500 m, that form the warm intermediate layer below the halocline along the transect. The salinity maximum of 34.9 with a temperature of −0.4°C corresponds to the cold, saline deep waters of the Canada Basin found below 2000 m.

The water mass composition of the study area, presented as pie charts in Figure 2a, is described below in section 4.1.1 and presented in further detail in the supporting information.

Table 1. Vertical Distribution of Silicic Acid ($Si(OH)_4$) Concentrations, Biogenic and Lithogenic Silica ($bSiO_2$ and $lSiO_2$) Concentrations ($lSiO_2$ at Selected Depths), and Dissolved Si Isotope ($\delta^{30}Si(OH)_4$) Values at Six Stations Sampled During the Canadian IPY-GEOTRACES Expedition in the Arctic Ocean During August–September 2009[a]

Station/Lat Long	Sampling Depth (m)	$[Si(OH)_4]$ ($\mu mol\ L^{-1}$)	$[bSiO_2]$ ($[lSiO_2]$) ($nmol\ L^{-1}$)	$\delta^{30}Si(OH)_4$ (‰)
S1	5	6.09	62.0	+2.21
S1 69.3°N 137.6°W	15	3.44	26.2	+2.52
	35	3.74	52.8	–
	50	10.63	158.5	+2.65
S2	3	4.42	17.0	–
70.0°N 138.3°W	15	3.21	4.5 (68.6)	–
	45	8.98	32.9	+2.26
	75	14.20	204.8	+2.11
	100	17.57	344.1	+2.01
	125	18.51	53.1	+2.00
	150	24.39	37.2	+1.94
	175	29.15	32	+1.90
	200	33.16	107.2	+1.95
L1	2	2.04	–	–
71.7°N 139.1°W	22	1.98	7.9 (35.5)	–
	50	2.58	19.9	–
	85	12.05	8.9 (33.7)	+2.02
	126	29.48	8.4 (75.3)	+1.73
	150	33.34	14.1	+1.76
	200	17.56	6.6	+1.91
	250	10.41	16.2 (93.9)	+2.08
	300	10.20	17.4	+1.87
	400	7.43	4.4	–
	500	7.24	–	+1.93
	800	7.10	15.1	–
	1000	7.32	–	–
	1200	7.93	16.6	–
	1399	8.92	–	+1.94
	1699	10.90	15	+1.85
L1.1	3	1.99	12.1	+2.76
72.3°N 136.4°W	10	2.02	27.5 (86.2)	+2.29
	25	2.07	26.1	–
	70	2.92	4.9 (39.5)	–
	115	22.30	14.4 (14.4)	+2.06
	140	29.48	6.3	+1.89
	175	36.41	16.3	+1.83
	200	29.26	11.4	+1.77
	250	9.01	8.7 (27.4)	+1.98
	300	8.07	–	+2.11
	350	6.89	–	+2.25
	400	6.76	9.4 (36.9)	+2.08
	450	6.79	–	+2.01
	500	6.44	–	+2.17
	600	6.85	–	+2.19
	800	6.83	8.6 (48.3)	+2.02
	1000	7.05	–	+2.15
	1400	8.46	7.6	+1.99
	1600	10.05	–	+1.98
	1800	11.46	3	+2.14
	2000	12.17	–	+1.90
	2250	13.07	–	+1.96
	2500	14.37	3.8	+2.09
L2	2.7	1.93	16.6	+2.64
74.4°N 137.2°W	10	1.90	19.1,	+2.91
	30	1.76	9.3	–
	55	2.66	21.7	–
	100	21.07	24.8	+1.82
	125	28.17	15.4	+1.70

Table 1. (continued)

Station/Lat Long	Sampling Depth (m)	$[Si(OH)_4]$ ($\mu mol\ L^{-1}$)	$[bSiO_2]$ ($[lSiO_2]$) ($nmol\ L^{-1}$)	$\delta^{30}Si(OH)_4$ (‰)
	150	29.95	17.5	+1.76
	200	18.61	19.5	+1.83
	250	8.56	5.1 (49.9)	+1.95
	300	7.52	–	+2.14
	400	6.60	6.9	+2.02
	500	6.35	–	+2.08
	600	8.78	–	+2.08
	800	6.96	2.5	+2.05
	1000	6.97	–	+1.91
	1200	7.46	18	+2.00
	1400	8.07	6.2	+2.01
	1600	9.04	–	+1.83
	1800	9.92	5.9	+1.71
	2000	10.99	–	+1.76
	2250	12.13	–	+1.72
	2500	12.69	5.8	+1.79
	2750	13.77	–	+1.78
	3000	13.48	–	+1.75
L3	3	2.29	6.7	+2.65
75.2°N 137.4°W	10	2.32	11.9 (47.5)	+2.60
	32	1.68	40.6	+3.08
	60	3.30	35.6	+2.79
	115	21.25	16.9	+1.90
	140	28.51	3.1	+1.71
	150	31.56	16.1	+1.84
	200	25.41	–	+1.71
	250	8.63	5.1	+1.79
	300	7.08	–	+1.77
	400	5.97	8.1	+1.94
	500	5.82	–	+1.93
	600	6.14	–	+2.07
	800	6.31	4	+1.87
	1000	6.58	–	+1.93
	1200	7.03	4.5	+2.07
	1400	7.57	–	+1.85
	1600	8.40	–	–
	1800	9.48	7.8	+1.98
	2000	10.34	–	+2.10
	2250	11.44	–	+1.91
	2500	12.02	5.1	+1.90
	2750	13.28	–	+1.86
	3000	13.05	6.7	+1.91

[a]Except for the $lSiO_2$ data, the data presented in this table also appear in Figures 3 and 4.

3.2. Dissolved and Particulate Silicon Concentrations

Silicic acid concentrations were generally $<5\ \mu mol\ L^{-1}$ above the halocline (top ~100 m) and $<15\ \mu mol\ L^{-1}$ throughout the rest of the water column, with the exception of a mid-depth maximum between 125 and 200 m depth within the upper halocline where concentrations reached $36\ \mu mol\ L^{-1}$ (Table 1 and Figure 3). Below the halocline, $Si(OH)_4$ concentrations increased with depth from $\sim 7\ \mu mol\ L^{-1}$ at 1000 m to $\sim 14\ \mu mol\ L^{-1}$ at 2500–3000 m (stations L1.1 to L3).

Biogenic SiO_2 concentrations were <41 nmol Si L^{-1} in the upper 100 m of the slope and Canada Basin (north of 71°N, stations L1 to L3) and higher in surface waters at coastal stations S1 and S2, with a maximum of 344 nmol Si L^{-1} at 100 m depth at station S2 (Figure 4a and Table 1). Concentrations of $bSiO_2$ were generally <10 nmol Si L^{-1} in deeper waters. In comparison, $lSiO_2$ concentrations were similar at coastal and oceanic stations with values between 14 and 94 nmol Si L^{-1} in the upper 800 m and often exceeded those of $bSiO_2$ (Table 1). Major sources of $lSiO_2$ include the Mackenzie River and sea ice.

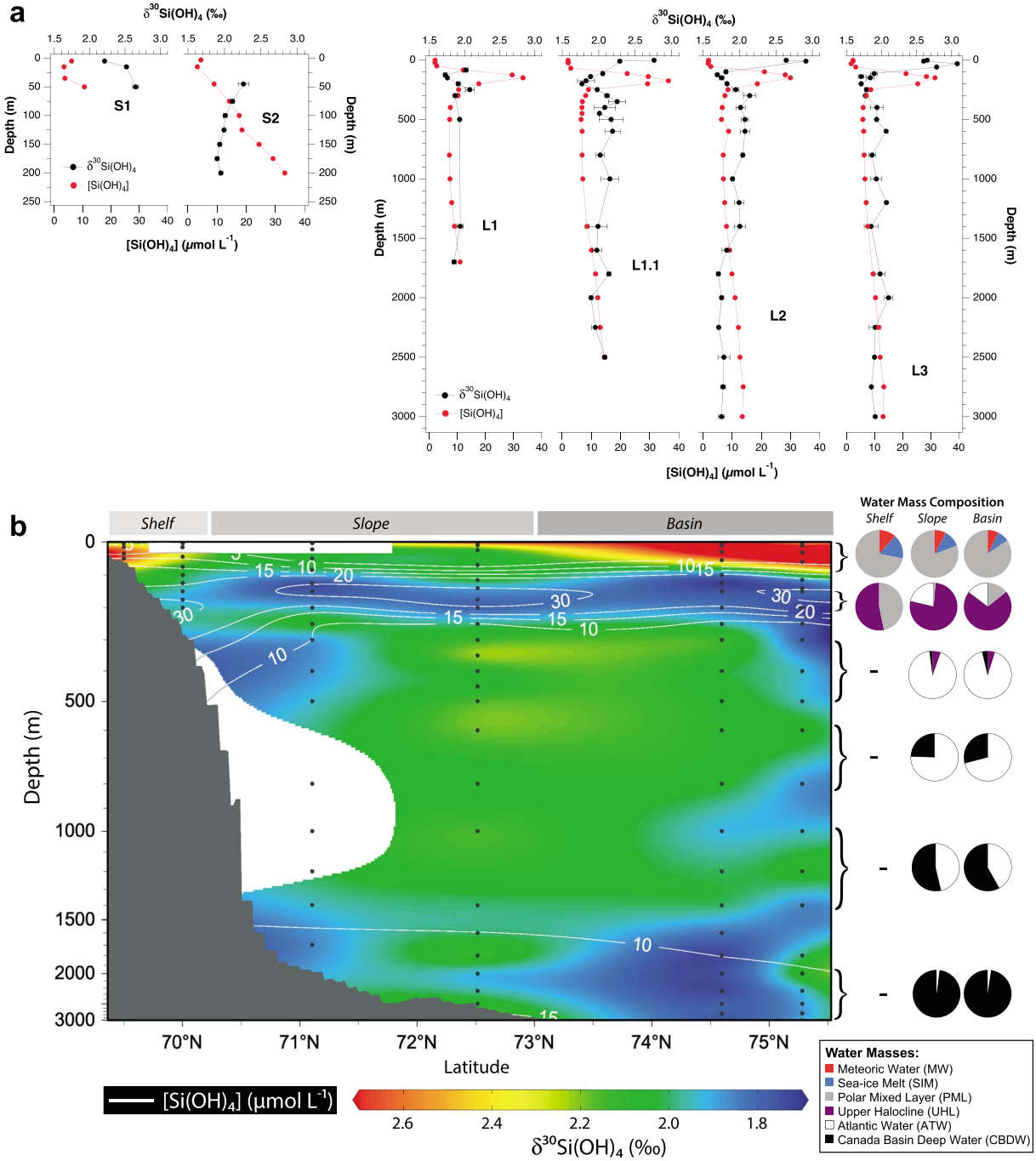

Figure 3. Silicic acid concentration, $[Si(OH)_4]$, and silicic acid isotopic composition, $\delta^{30}Si(OH)_4$, along the study section. (a) Discrete depth profiles of $Si(OH)_4$ and $\delta^{30}Si(OH)_4$ for all six stations. Symbols represent the mean ±1 SD of duplicate or triplicate measurements of the same field sample. (b) Vertical and latitudinal distribution of $Si(OH)_4$ (contour lines) and $\delta^{30}Si(OH)_4$ (color contours). As in Figure 1, pie charts represent the water mass composition for the shelf, slope, and basin waters over the depth ranges indicated by brackets (see supporting information). The shelf, slope, and basin waters are indicated by the grey bars along the top of Figure 3b. Black dots indicate the sampling depths for $[Si(OH)_4]$. Sampling locations for $\delta^{30}Si(OH)_4$ are the same as those for $[Si(OH)_4]$, with the exception of fewer depths sampled for $\delta^{30}Si(OH)_4$ in the upper 100 m and the lack of $\delta^{30}Si(OH)_4$ data within this depth range for stations S2 and L1 (Figure 3a and white box in Figure 3b).

3.3. Distribution of Silicon Isotopes

Vertical profiles of $\delta^{30}Si(OH)_4$ revealed the highest (heaviest) values in surface waters (top ~ 100 m), consistent with fractionation during diatom growth (Figures 3a and 3b). The mean $\delta^{30}Si(OH)_4$ for the upper 60 m at these profile stations was quite high, +2.60 ± 0.27‰ ($n = 11$) (note the lack of data in the upper 100 m

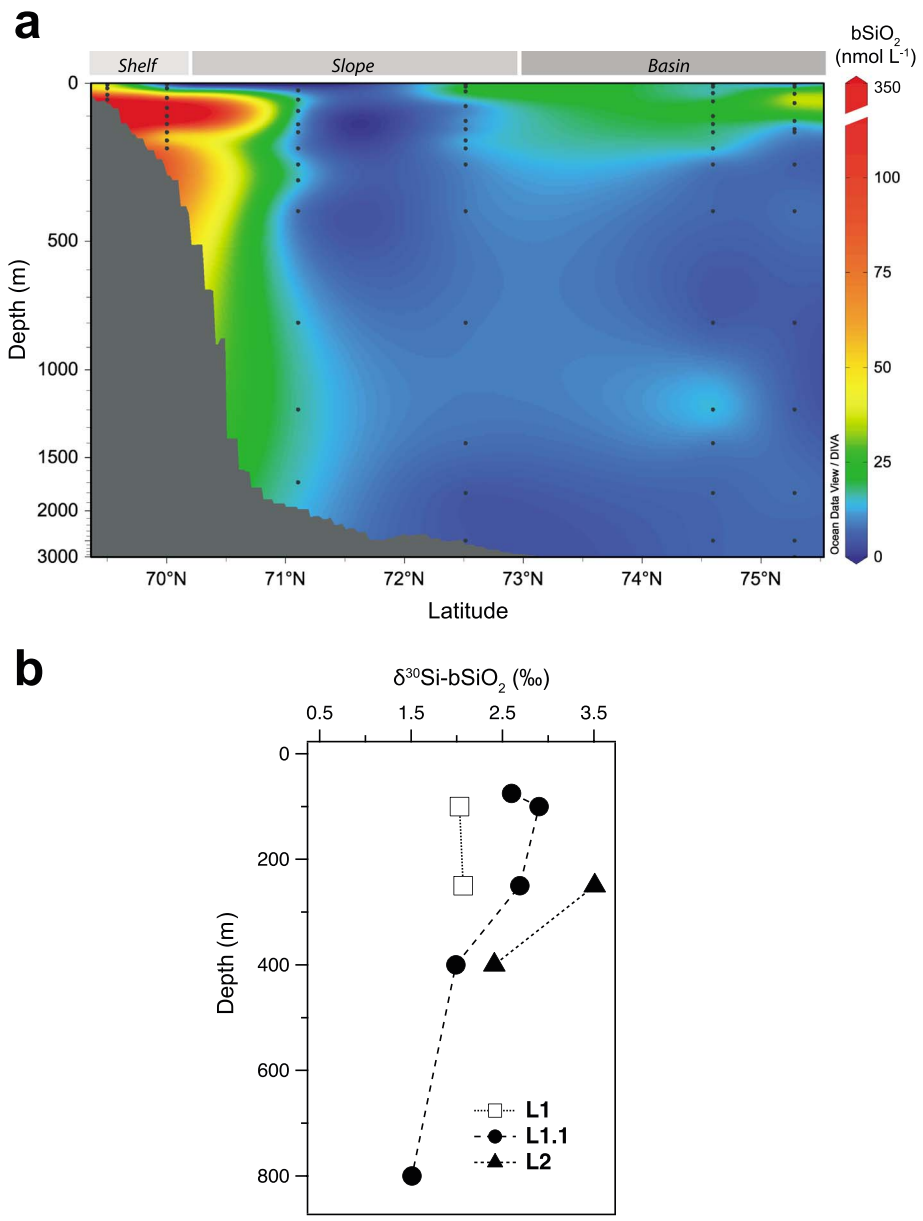

Figure 4. Biogenic silica concentration, [$bSiO_2$], and biogenic silica Si isotopic composition, δ^{30}Si-$bSiO_2$, along the sampling section. (a) Vertical and latitudinal distribution of $bSiO_2$ concentrations. The shelf, slope, and basin waters are indicated by the grey bars along the top of this panel. (b) Discrete depth profiles of δ^{30}Si-$bSiO_2$ at stations L1, L1.1, and L2.

at stations S2 and L1, Figure 3a). These high values at the surface were confirmed by the $\delta^{30}Si(OH)_4$ values from the underway collection system (at ~7 m) that were between +2.63‰ and +2.76‰, averaging +2.73 ± 0.08‰ ($n = 7$, Table 2). Positive $\delta^{30}Si(OH)_4$ values were observed throughout the water column, ranging from +1.70‰ to +3.08‰ (Table 1 and Figures 3a and 3b). Subsurface maxima in $\delta^{30}Si(OH)_4$ were observed at 3–30 m depth at stations L1.1, L2 and L3 (Figure 3a). The profiles for stations L1 to L3 contained a local minimum within the halocline of between +1.70‰ and +1.80‰ associated with the $Si(OH)_4$ maximum at ~125–200 m. The highest subsurface $\delta^{30}Si(OH)_4$ values (> +2.00‰) were observed below the halocline between 250 and ~500 m (Figure 3 and Table 1). Isotope values decreased at depths >2000 m but remained higher than ever measured for oceanic deep waters, averaging +1.88‰ ± 0.12‰ (Figure 3 and Table 1). Water mass composition indicated in Figure 2a is included again in Figure 3b to allow comparison with $\delta^{30}Si(OH)_4$ signals.

Table 2. Latitudinal Distribution of Si Isotope Values for Silicic Acid ($\delta^{30}Si(OH)_4$) and Biogenic Silica ($\delta^{30}Si\text{-}bSiO_2$) for Surface Waters (~7 m Depth) From the Underway Sampling Collection System, and the 5-Day Mean Sea-Ice Concentration (% of Ocean Surface Area)[a]

Location Name	Latitude (°N)	Longitude (°W)	$\delta^{30}Si(OH)_4$ (‰)	$\delta^{30}Si\text{-}bSiO_2$ (‰)	5-Day Mean Sea-Ice Concentration (%)
A.4	70.43	138.44	-	+2.00	6.8
A.7	71.07	139.18	-	+2.02	14.8
A.8	71.15	139.11	-	+2.33	15.7
A.9	72.27	139.19	+2.75	+2.49	39.6
A.10	73.56	139.4	-	+2.38	47.9
A.11	74.39	137.22	+2.64	+3.17	61.6
A.12	74.35	137.07	+2.65	+3.06	73.8
A.13	74.24	136.26	+2.89	+2.86	76.7
A.15	75.36	133.22	-	+3.04	77.3
A.18	75.19	137.37	+2.65	+2.98	86.3
A.19	75.16	137.44	+2.63	+2.91	86.8
A.20	74.29	136.59	+2.74	+3.42	87.2
A.22	72.3	136.35	+2.76	+2.62	90.0
A.23	71.29	136.35	+2.69	+2.56	92.5
A.24	72.8	136.45	+2.66	+3.15	94.8
A.26	71.17	134.33	+2.74	+2.46	99.8

[a]The 5-day mean sea-ice concentration was derived with the ASI algorithm and brightness temperature data from the Advanced Microwave Scanning Radiometer aboard the EOS satellite (AMSR-E). Data presented in this table are also shown in Figure 6.

The Si isotopic composition of $bSiO_2$ was also among the heaviest measured in the ocean to date. The surface (~7 m) $\delta^{30}Si\text{-}bSiO_2$ values from samples obtained from the underway system ranged from +2.00‰ to +3.42‰ along the section (Table 2). Similarly, depth profiles of $\delta^{30}Si\text{-}bSiO_2$ showed high values in the upper 400 m of the water column (+2.03‰ to +3.51‰) with values decreasing with depth to +1.51‰ at 800 m (Figure 4b).

4. Discussion

4.1. Mechanisms Controlling Silicon Isotopic Distribution

4.1.1. Relationship Between $\delta^{30}Si(OH)_4$ and Water Mass Distribution

Comparison of the isotope distributions with that of major water masses confirms a close association between the distributions of $\delta^{30}Si(OH)_4$ signals and the water masses identified in the study area. *Carmack et al.* [1989] and *Macdonald et al.* [1989, 2002] described six main water masses present in this region as end-members: (1) Meteoric Water (MW, Mackenzie River water and precipitation), (2) Sea Ice Melt (SIM), (3) Polar Mixed Layer (PML), (4) Upper Halocline Water (UHL, composed mainly of modified Pacific waters), (5) Atlantic Water (ATW), and (6) Canada Basin Deep Water (CBDW). The pie charts in Figures 2a and 3b show the average relative contribution of these water masses on the shelf, on the continental slope, and in the deep basin over the indicated depth ranges along the study section. Water mass distributions were determined using an optimum multi-parameter (OMP) analysis (see supporting information).

Lansard et al. [2012] described the PML as the nearly homogenous winter surface water that is modified through the addition of MW and SIM during summer and through removal of SIM in winter. During this study, the low-salinity surface layer (0–100 m) consisted primarily of PML with small contributions from MW and SIM at depths less than ~70 m (Figures 2a and S1a–S1c in the supporting information). MW and SIM are only present in surface waters ($<$100 m) and their contributions decrease with distance from shore (Figures 2a and S1a and S1b). $\delta^{30}Si(OH)_4$ signals begin to decline below ~50 m with the shift from MW and SIM to UHL (Figures 3 and S1a–S1d).

The minimum in $\delta^{30}Si(OH)_4$ between 125 and 250 m is located within the UHL and is therefore associated with the relatively cold waters of Pacific origin. Waters in the UHL are derived from the Bering Sea in the Pacific Ocean [*Jones and Anderson,* 1986; *Carmack et al.,* 1989; *McLaughlin et al.*, 1996] but are modified by biological consumption and remineralization while they transit over shallow Arctic shelves [*Jones and Anderson,* 1986]. Nevertheless, despite the nutrient alteration of these waters within the Arctic, they still maintain geochemical signals (e.g., nitrate to phosphate ratios) that indicate a Pacific origin [*Simpson et al.*, 2008].

Table 3. Water Mass $\delta^{30}Si(OH)_4$ Signatures, Temperature, and Salinity for the Study Region[a]

		Water Mass Values Derived From:						
		Literature, Model, and *T-S* Analysis			Measured Parameters[i] (This Study)			
Water Mass[b]	Depth Range (From OMP)[c]	$\delta^{30}Si(OH)_4$ (‰)	Temperature[d] (°C)	Salinity[d]	$\delta^{30}Si(OH)_4$ (‰)	Temperature[d] (°C)	Salinity[d]	*n*
Meteoric Water (MW)	0–10 m	+1.36[e]	+10	0	na[j]	na[j]	na[j]	-
Sea Ice Melt (SIM)	0–20 m	+1.9[f]	0	4.7	na[j]	na[j]	na[j]	-
Polar Mixed Layer (PML)	50–100 m	na[g]	−0.70	32.0	+2.26 ± 0.39	−0.88 ± 0.42	31.2 ± 0.67	6
Upper Halocline Layer (UHL)	125–200 m	na[g]	−1.44	33.1	+1.84 ± 0.10	−1.44 ± 0.03	32.9 ± 0.03	3
Atlantic Water (ATW)	350–500 m	na[g]	+0.80	34.8	+2.04 ± 0.11	+0.66 ± 0.07	34.8 ± 0.02	7
Canada Basin Deep Water (CBDW)	>2,000 m	+1.84[h]	−0.40	34.9	+1.88 ± 0.12	−0.38 ± 0.03	34.9 ± 0.01	13

[a]Values are obtained from literature results, model (this study) and *T-S* analysis of this data set, and compared to those measured from samples obtained at depths where ≥ 90% of a single water mass existed according to the OMP-derived water mass distributions (see supporting information).
[b]Water masses as defined by *Carmack et al.* [1989] and *Macdonald et al.* [1989, 2002].
[c]Depth ranges for PML, UHL, ATW, and CBDW correspond to where ≥ 90% of a single water mass is found according to OMP water mass analysis (see supporting information). The depth range for the MW and SIM water types corresponds to where 8–21% of these water masses were found according to the OMP water mass analysis, as these water masses never contributed more than 21% to the total water mass composition at any of our sampling depths.
[d]Values based on a *T-S* analysis of the GEOTRACES data set (see supporting information).
[e]Value from *Pokrovsky et al.* [2013].
[f]Value from *Fripiat et al.* [2013].
[g]na: Data not available. The $\delta^{30}Si(OH)_4$ signals of these water masses have never been measured or estimated before this study.
[h]Calculated from the PANDORA model, see section 4.2 (this study).
[i]All values are the mean (± SD) of each parameter from all sampling depths where ≥ 90% of a single water mass existed according to the OMP-derived water mass distributions.
[j]na: Data not available. The $\delta^{30}Si(OH)_4$, *T*, and *S* signals of these water masses could not be estimated using the OMP water mass data as the water masses never contributed more than 21% to the total water mass composition at any of our sampling depths.

At deeper depths, the maximum in $\delta^{30}Si(OH)_4$ between 350 and 500 m is associated with nearly pure ATW, which is warmer and more saline than the UHL. $\delta^{30}Si(OH)_4$ signals are either fairly constant or decrease slightly with depth between 600 and 2000 m as CBDW displaces ATW (Figure 3b). $\delta^{30}Si(OH)_4$ values decline below 2000 m where the cold and more saline CBDW accounts for >90% of the water present in samples from this depth zone (Figure 3 and supporting information).

4.1.2. Estimates of the $\delta^{30}Si(OH)_4$ of Dominant Water Masses

The OMP analysis reveals a strong dominance of the PML, UHL, ATW, or CBDW in subsets of our samples allowing us to estimate the isotopic composition of these specific water masses. The mean $\delta^{30}Si(OH)_4$ value for all depths ($n = 6$) where the percentage of PML was >90% was +2.26 ± 0.39‰ (Table 3). As PML resides in the euphotic zone, this value is likely modulated by fractionation during biosilicification in surface waters. We did not calculate the $\delta^{30}Si(OH)_4$ signatures of MW or SIM as these water masses never comprised more than 21% of the water present in any of our samples. Nevertheless, previously published work that directly measured the signals in these water masses report $\delta^{30}Si(OH)_4$ of +1.36 ± 0.19‰ for MW [*Pokrovsky et al.,* 2013] and +1.9 ± 0.1‰ for SIM [*Fripiat et al.,* 2013], although there is some uncertainty with these values.

The $\delta^{30}Si_{MW}$ signal from *Pokrovsky et al.* [2013] comes from a summertime measurement of Mackenzie River water (the main component of MW in our study region), and thus, this signal is likely representative of the MW water mass during the time when our study took place. This value also falls within the range of annual discharge-weighted $\delta^{30}Si(OH)_4$ of two Siberian rivers (+1.08 to +1.67‰) and for summertime $\delta^{30}Si(OH)_4$ measurements for other large Arctic rivers (+1.17 to +2.30‰ for the Lena, Yennissey and Ob) [*Pokrovsky et al.,* 2013]. However, *Pokrovsky et al.* [2013] detected a significant seasonal variability in the $\delta^{30}Si(OH)_4$ signatures of two Siberian rivers, with much lower $\delta^{30}Si(OH)_4$ values during high water events, such as the spring flood, compared to later in the summer. These changes can result in differences between summertime measurements of $\delta^{30}Si(OH)_4$ and annual discharge-weighted $\delta^{30}Si(OH)_4$ of up to 1‰.

The $\delta^{30}Si_{SIM}$ value of +1.9 ± 0.1‰ from *Fripiat et al.* [2013] represents the wintertime $\delta^{30}Si(OH)_4$ composition of sea ice prior to the onset of the productive period (March), whereas our study was conducted near the end of the summer (August/September). As the seasonally productive period progresses, the $\delta^{30}Si(OH)_4$ of sea ice will increase from its baseline wintertime value with increasing consumption of brine $Si(OH)_4$ by sea-ice diatoms, which tend to dominate sea-ice primary production [*Gosselin et al.,* 1997]. By the end of the summer, the value for $\delta^{30}Si_{SIM}$ could reach a maximum close to +2.9‰, assuming a $^{30}\varepsilon = -1.0$‰ (average from

De La Rocha et al. [1997] and *Sutton et al.* [2013]) and complete exhaustion of the available $Si(OH)_4$ pool. Thus, it is likely that $\delta^{30}Si_{SIM}$ for our region/study period falls somewhere in the range of +1.9 to +2.9‰ depending on the extent of $bSiO_2$ production, dissolution and export. *Fripiat et al.* [2007] report a similar $\delta^{30}Si(OH)_4$ range of +1.8 to +2.3‰ for productive first-year sea ice in the Antarctic.

Between 125 and 250 m depth, the average $\delta^{30}Si(OH)_4$ value from samples with >90% UHL was +1.84 ± 0.10‰ (Table 3). This UHL water mass, composed of modified Pacific water, is characterized by low temperatures (minimum of ~ −1.44°C, Table 3) and $Si(OH)_4$ concentrations exceeding 30 μmol L^{-1} (Table 1). High concentrations of $Si(OH)_4$ usually translate into relatively low $\delta^{30}Si(OH)_4$, consistent with our observations on all off-shelf profiles: a minimum in $\delta^{30}Si(OH)_4$ corresponding to the depth of the $[Si(OH)_4]$ maximum (Figure 3). The $\delta^{30}Si(OH)_4$ minimum observed within this depth interval is only ~0.3‰ on average from waters immediately above and below the UHL (Figure 3 and Table 3). Although no data currently exist for the Pacific end-member at the Bering Strait, *Reynolds et al.* [2006] report a $\delta^{30}Si(OH)_4$ value of about +1.0‰ and $[Si(OH)_4]$ of ~23 μmol L^{-1} for waters at 50°N, 167°W (approximately 1800 km south from the Bering Strait). Our higher isotope values and $[Si(OH)_4]$ suggest a significant alteration of waters of Pacific origin present in the Canada Basin, in agreement with *Jones and Anderson*'s [1986] findings that waters over the Arctic shelves are exposed to strong nutrient remineralization and later advected into the central Arctic.

The ATW, which enters the Arctic Ocean through the Barents Sea and Fram Strait, is observed below the UHL. ATW is primarily found between 350 and 500 m depth, with the water mass contribution reaching a maximum of ~90% between 400 and 450 m (Figure 2a). In the North Atlantic, this water has a $[Si(OH)_4]$ of ~11 μmol L^{-1} and an Si isotopic value of +1.55% [*de Souza et al.*, 2012a]. As this water cools during travel through the Arctic Ocean, it loses buoyancy and sinks under both the mixed layer and the UHL [*Grebmeier et al.*, 2006] to form the ATW water mass. The ATW that we observe around 400 m depth along our sampling transect has a mean $[Si(OH)_4]$ of 6.7 ± 0.5 μmol L^{-1} (Table 1) and a $\delta^{30}Si(OH)_4$ value of +2.04 ± 0.11‰ (Table 3), implying that this water mass has experienced dilution due to mixing with other water masses and/ or nutrient drawdown through biological uptake compared to the North Atlantic end-member.

Waters below ~2000 m in the Canada Basin are comprised almost entirely (>90%) of CBDW, which forms through convection of modified Atlantic water [*Carmack and Wassmann,* 2006]. We calculated a mean $\delta^{30}Si(OH)_4$ signature of +1.88 ± 0.12‰ for CBDW (Table 3), which is the most positive $\delta^{30}Si(OH)_4$ value measured in deep waters anywhere in the global ocean. The CBDW water mass is isolated from other deep water masses by the Alpha, Lomonosov and Mendeleev Ridges that rise from the ocean floor to 400 to 1500 m below sea level and also separate the Canada Basin from the Makarov and Eurasian Basins (Figure 1a). Therefore, the CBDW experiences low exchange and has a residence time of 450–500 years in the Canada Basin [*Macdonald et al.*, 1993]. The mechanisms leading to the heavy $\delta^{30}Si(OH)_4$ values in CBDW and ATW are discussed below (section 4.2).

4.1.3. Influence of the Mackenzie River

The influence of the Mackenzie River on $\delta^{30}Si(OH)_4$ values is clearly evident, although it was mainly limited to the upper 25 m on the shelf and slope and decreased with distance from shore. The lightest surface $\delta^{30}Si(OH)_4$ value (+2.21‰, 5 m at S1) was measured in the sample with the largest contribution from MW (~18%) (Figure 3), consistent with the relatively low $\delta^{30}Si(OH)_4$ of the Mackenzie River (+1.36 ± 0.19‰) [*Pokrovsky et al.*, 2013] and the $\delta^{30}Si(OH)_4$ range of +1.17 to +2.30‰ for the large Arctic rivers Lena, Yenissey, Ob, and Mackenzie [*Pokrovsky et al.*, 2013]. Surface water isotope values should decrease with increasing contribution from MW. Indeed, we found a negative correlation ($R^2 = 0.43$, $p < 0.005$) between surface (0–30 m) $\delta^{30}Si(OH)_4$ values and %MW along the entire sampling region (Figure 5), although the R^2 of this regression decreases to 0.14 (insignificant at $p > 0.15$) when removing the single data point with high %MW (~18%). On the other hand, the removal of this data point has no significant effect on the slope or intercept of the line.

4.1.4. Estimating the Biogenic ^{30}Si Fractionation Factor

Using our water mass $\delta^{30}Si(OH)_4$ results, we estimated the biologically-driven ^{30}Si fractionation factor, $^{30}\varepsilon$, in surface waters (0–125 m) using two simple models. The first model assumes a closed system where nutrient consumption at the surface is not replenished by external sources and is described by the Rayleigh distillation equation:

$$\delta^{30}Si(OH)_{4,\ observed} = \delta^{30}Si(OH)_{4,source} + {}^{30}\varepsilon\ \ln\ f \quad (2)$$

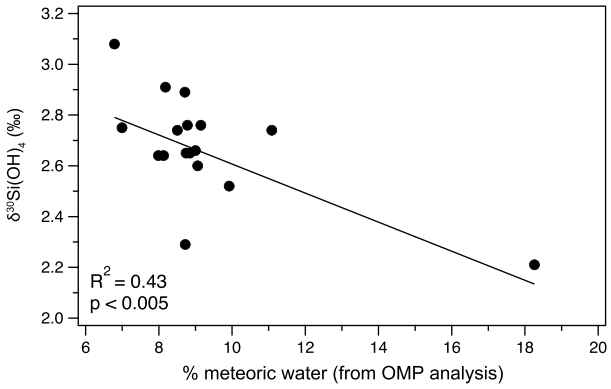

Figure 5. Surface water (0–30 m) $\delta^{30}Si(OH)_4$ values from depth profiles and underway samples versus the contribution of Mackenzie River water (% meteoric water, MW) along the entire sampling area. The % MW for the $\delta^{30}Si(OH)_4$ profile data was determined based on the OMP water mass analysis. For the underway $\delta^{30}Si(OH)_4$ data, the %MW was determined using a surface contour plot of the %MW at 5 m and 2-D interpolation based on the latitude and longitude of sampling.

The second model assumes an open or steady state system, where there is a continuous supply of nutrients from external sources to surface waters balanced by the continuous removal of nutrients via biological consumption. In other words, the model assumes that the overall concentration of nutrients in the surface is constant (i.e., inputs = outputs) and can be described by the following equation:

$$\delta^{30}Si(OH)_{4,observed} = \delta^{30}Si(OH)_{4,source} + {}^{30}\varepsilon(1-f) \quad (3)$$

In equations (2) and (3), $\delta^{30}Si(OH)_{4,observed}$ is equal to our measured $\delta^{30}Si(OH)_4$, and $\delta^{30}Si(OH)_{4,source}$ is equal to the source water $\delta^{30}Si(OH)_4$ calculated based on the relative contributions of each water mass and their associated $\delta^{30}Si(OH)_4$ values as

$$\delta^{30}Si(OH)_{4,source} = \%MW \times \delta^{30}Si_{MW} + \%SIM \times \delta^{30}Si_{SIM} + \%PML \times \delta^{30}Si_{PML} \quad (4)$$

For equation (4), we use a value of +1.36‰ for $\delta^{30}Si_{MW}$ [*Pokrovsky et al.,* 2013], +1.9‰ for $\delta^{30}Si_{SIM}$ [*Fripiat et al.,* 2013], and +2.26‰ for $\delta^{30}Si_{PML}$ (Table 3).

For equations (2) and (3), *f* is described as

$$f = \left[Si(OH)_4\right]_{observed} / \left[Si(OH)_4\right]_{source} \quad (5)$$

The $[Si(OH)_4]_{source}$ is equal to the expected source water $[Si(OH)_4]$ as derived from the relative contribution of each water mass and their associated initial $[Si(OH)_4]$ (i.e., before any localized Si consumption):

$$\left[Si(OH)_4\right]_{source} = \%MW \times \left[Si(OH)_4\right]_{MW} + \%SIM \times \left[Si(OH)_4\right]_{SIM} + \%PML \times \left[Si(OH)_4\right]_{PML} \quad (6)$$

with initial concentrations of $[Si(OH)_4]_{MW} = 40–56\ \mu mol\ L^{-1}$ based on two independent measurements of the Mackenzie river $[Si(OH)_4]$ by *Simpson et al.* [2008], $[Si(OH)_4]_{SIM} = 3.2–9.4\ \mu mol\ L^{-1}$ calculated from *Fripiat et al.* [2013] by accounting for the salinity normalization of $[Si(OH)_4]$ and brine volume, and $[Si(OH)_4]_{PML} = 20\ \mu mol\ L^{-1}$ from *Carmack et al.* [2004].

For surface waters, we calculated a mean (±1 SD) ${}^{30}\varepsilon$ of -0.33 ± 0.05‰ using the closed system model (equation (2)) and -0.97 ± 0.17‰ using the open system model (equation (3)). Since MW and SIM combined only contribute 31% or less to the total water mass, our estimates of ${}^{30}\varepsilon$ are relatively insensitive to the $[Si(OH)_4]$ chosen for SIM and MW in equation (6) (≤0.03‰ difference in ${}^{30}\varepsilon$ over the range of values cited above). Laboratory-based measurements of this fractionation factor are -1.1 ± 0.4‰ for three diatom strains [*De La Rocha et al.,* 1997] and -0.98 ± 0.5‰ (-0.53‰ to -2.09‰) for nine diatom strains [*Sutton et al.*, 2013]. Field-based estimates vary between -1.0‰ (closed system) and -1.7‰ (open system) in Antarctic waters [*Varela et al.*, 2004], with an average of -1.2 ± 0.3‰ [*De La Rocha et al.*, 2000, 2011; *Varela et al.*, 2004; *Cardinal et al.*, 2005; *Reynolds et al.*, 2006; *Beucher et al.*, 2008; *Cavagna et al.*, 2011; *Fripiat et al.*, 2011b]. The value of ${}^{30}\varepsilon$ calculated for our study using the closed system model is significantly different from laboratory estimates of ${}^{30}\varepsilon$ (*t* test, $p < 0.0001$ from both *De La Rocha et al.* [1997] and *Sutton et al.* [2013]) and much lower than average field-based estimates from other parts of the global ocean. In contrast, the value of ${}^{30}\varepsilon$ calculated using the open system model does not differ significantly from laboratory estimates (*t* test, $p > 0.2$ from both *De La Rocha et al.* [1997] and *Sutton et al.* [2013]) and is comparable to the average field-based estimate of ${}^{30}\varepsilon$ derived from previous studies. Given these results, it appears that the open system model is the most applicable to our study. Nevertheless, the seasonal drawdown of $Si(OH)_4$ observed in this region [*Simpson et al.,* 2008; *Tremblay et al.,* 2008] suggests that the closed system model would be a more suitable representation of the $\delta^{30}Si$ dynamics, even when our closed system ${}^{30}\varepsilon$ estimate does not agree with previous field and laboratory observations.

A possible explanation for this discrepancy is that the overall expression of $^{30}\varepsilon$ is low (closed system model) because a large part of the seasonal $Si(OH)_4$ drawdown occurred in sea ice. Assuming that sea ice has a limited exchange with the underlying ocean and that a significant portion of primary production occurs in sea ice [*Gosselin et al.,* 1997; *Fernández-Méndez et al.*, 2015], the isotope systematics of the sea ice/water column system can be thought of in a manner similar to that for denitrification in pelagic/sedimentary systems. In these systems, the apparent isotope effect for denitrification, ε_{app}, is much smaller than the cellular isotope effect, ε_{cell}, because a significant portion of this process occurs in the sediments, which are diffusion limited (i.e., limited exchange with the overlying ocean). Assuming that the Si isotope systematics of the sea ice/water column system resemble those of pelagic/sedimentary denitrification, an overall $^{30}\varepsilon$ can be calculated based on the relative proportions of primary production between sea ice and the water column and an estimate of the apparent $^{30}\varepsilon$ for each system. For example, if 60% of the primary production occurs in sea ice [e.g., *Gosselin et al.*, 1997] with the extreme assumption that diatom growth in ice results in no apparent fractionation, $^{30}\varepsilon_{app} = 0.0‰$, and the remaining 40% of primary production occurs in the water column with a $^{30}\varepsilon = -1.02 \pm 0.42‰$ ($n = 14$, average from *De La Rocha et al.* [1997] and *Sutton et al.* [2013]), the overall $^{30}\varepsilon$ ($=0.6 \times 0.0‰ + 0.4 \times -1.02‰$) is $-0.41 \pm 0.16‰$ (or $-0.47 \pm 0.06‰$ using the field $^{30}\varepsilon$ estimate of $-1.2 \pm 0.16‰$). This overall $^{30}\varepsilon$ is not significantly different ($p > 0.06$) from our closed system estimate of $^{30}\varepsilon$ of $-0.33 \pm 0.05‰$.

In summary, whereas our calculation of $^{30}\varepsilon$ using an open system model produces a value similar to that estimated for other parts of the global ocean, this model is not necessarily representative of the dynamics of our study region. The seasonal drawdown of $Si(OH)_4$ observed in previous studies [*Simpson et al.,* 2008; *Tremblay et al.,* 2008] suggests that this region is better represented by a closed system model, although the estimate of $^{30}\varepsilon$ from this model is much lower than expected. The existence of productive overlying sea ice complicates the interpretation of the isotope systematics, but, when accounted for, the estimate of $^{30}\varepsilon$ is not significantly different from our closed system value of $^{30}\varepsilon$. These results indicate that caution is required when selecting the most appropriate isotope model to describe a system.

4.1.5. Effects of Silica Dissolution

Fractionation during $bSiO_2$ dissolution preferentially releases the lighter isotopes of Si [*Demarest et al.,* 2009], which, to first order, would act to decrease $\delta^{30}Si(OH)_4$ and increase $\delta^{30}Si\text{-}bSiO_2$. Detecting the effect of $bSiO_2$ dissolution on $\delta^{30}Si(OH)_4$ is difficult due to the low biomass and low $[bSiO_2]/[Si(OH)_4]$ observed along the section and the lack of knowledge of the vertical distribution of $bSiO_2$ dissolution rates within the water column. In contrast, the effects of dissolution on $\delta^{30}Si\text{-}bSiO_2$ are analytically easier to detect and should be revealed from the change in $\delta^{30}Si\text{-}bSiO_2$ values with depth as sinking particles dissolve. Although the loss of lighter isotopes of Si should lead to increasing $\delta^{30}Si\text{-}bSiO_2$ with depth, an opposite pattern was observed in our data (Figure 4b), with a decline in $\delta^{30}Si\text{-}bSiO_2$ of 1.18‰ between 250 and 800 m at station L1.1.

Buckley et al. [2010] observed similar declines of $\delta^{30}Si\text{-}bSiO_2$ in particles captured by sediment traps deployed at 250 and 800 m depth in the Cariaco Basin over a 10-month time series. It is difficult to reconcile these patterns if fractionation during dissolution preferentially releases lighter isotopes from sinking opal. It is possible that SiO_2 dissolution is not congruent among siliceous particles. This could mask the effects of fractionation during dissolution if dissolution results in the near-complete loss of $bSiO_2$ in lightly silicified particles, while others survive the transit to depth relatively intact. Such a mechanism would produce relatively uniform vertical $\delta^{30}Si\text{-}bSiO_2$ profiles, as have been observed in the Southern Ocean [*Fripiat et al.,* 2011b], but it would not account for the shape of our $\delta^{30}bSiO_2$ profiles (Figure 4b). We argue below (section 4.1.6) that the observed decrease in $\delta^{30}Si\text{-}bSiO_2$ with depth in the Canada Basin may be the result of a relatively recent input of isotopically heavy sea-ice diatoms to surface waters.

4.1.6. Possible Effect of Sea-Ice Diatoms on $\delta^{30}Si\text{-}bSiO_2$

Surface water $\delta^{30}Si\text{-}bSiO_2$ increases significantly with increasing latitude ($R^2 = 0.63$, $p < 0.0002$; Figure 6a) and sea-ice concentration ($R^2 = 0.60$, $p < 0.0004$; Figure 6b). A similar correlation between $\delta^{30}Si(OH)_4$ and these parameters would be expected if all $bSiO_2$ production occurred within the water column. However, $\delta^{30}Si(OH)_4$ signals remained fairly constant with increasing latitude and sea-ice concentration ($R^2 = 0.02$, $p < 0.71$ and $R^2 = 0.0002$, $p < 0.97$, respectively). An increase in $\delta^{30}Si\text{-}bSiO_2$ without a concomitant effect on $\delta^{30}Si(OH)_4$ implies that suspended $\delta^{30}Si\text{-}bSiO_2$ signals may be influenced by a source outside the surface planktonic system. One possibility is the input of sea-ice diatoms, which can have a much heavier

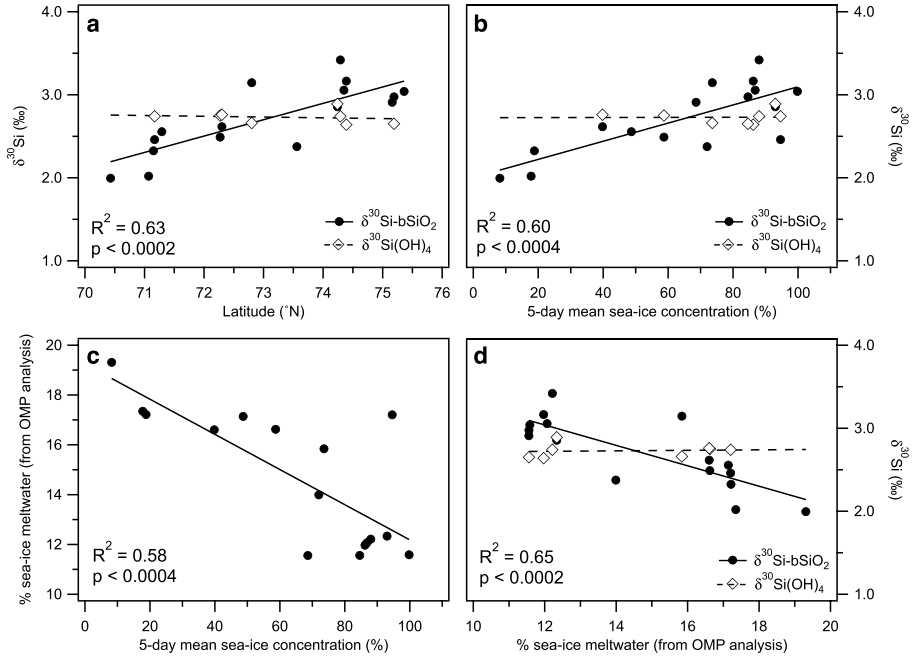

Figure 6. (a) Latitudinal distribution of underway (~7 m) δ^{30}Si-bSiO$_2$ and δ^{30}Si(OH)$_4$, (b) underway δ^{30}Si-bSiO$_2$ and δ^{30}Si(OH)$_4$ versus 5-day mean sea-ice concentration (%) calculated for each underway sampling location, (c) contribution of sea-ice meltwater (%SIM) to surface waters, determined using a surface contour plot of the %SIM at 5 m and 2-D interpolation based on the latitude and longitude of the underway samples, versus the 5-day mean sea-ice concentration (%, same data as shown in Figure 6b), and (d) underway δ^{30}Si-bSiO$_2$ and δ^{30}Si(OH)$_4$ versus %SIM (as determined in Figure 6c) in surface waters. Statistical R^2 and p values shown in Figure panels 6a, 6b, and 6d are for the relationships with δ^{30}Si-bSiO$_2$.

δ^{30}Si-bSiO$_2$ signature than do planktonic diatoms. *Fripiat et al.* [2007] measured a δ^{30}Si-bSiO$_2$ from sea-ice diatoms that was ~ +0.5‰ more positive than the suspended bSiO$_2$ from the adjacent mixed layer.

As sea ice melts, there should be an increased contribution of SIM to surface waters (i.e., a negative relationship between %SIM and sea-ice concentration) with a concomitant increase in the flux of isotopically heavy sea-ice diatoms to the pelagic diatom assemblage (i.e., a positive correlation between %SIM and δ^{30}Si-bSiO$_2$). Although we observe a significant negative relationship between %SIM and the 5-day mean sea-ice concentration ($R^2 = 0.58$, $p < 0.0004$, Figure 6c), δ^{30}Si-bSiO$_2$ is negatively correlated with %SIM ($R^2 = 0.65$, $p < 0.0002$, Figure 6d), opposite to the positive relationship expected. One possible explanation for this unexpected relationship is that the residence time of SIM in surface waters is confounding any link between δ^{30}Si-bSiO$_2$ and %SIM. The %SIM gives no indication of its residence time in surface waters, which could range from minutes to weeks or longer. Combined with the propensity for sea-ice diatoms to form fast sinking aggregates [e.g., *Riebesell et al.*, 1991], any sea-ice diatoms supplied to surface waters through sea-ice melting may have already sunk out. In this case, sea-ice concentration would be a better predictor of the sea-ice diatom flux provided that the sea ice is melting, not forming. This is a reasonable scenario given the sampling period (late August/early September). Based on the correlation between δ^{30}Si-bSiO$_2$ and latitude (Figure 6a) as well as δ^{30}Si-bSiO$_2$ and sea-ice concentration (Figure 6b), it is reasonable to assume that an increasing contribution of sea-ice diatoms to the pelagic diatom assemblage in regions of higher ice cover will lead to higher δ^{30}Si-bSiO$_2$ values in surface waters, masking the expected δ^{30}Si-bSiO$_2$ trends with depth.

4.2. Modeling the Si Isotopic Composition of the Arctic Ocean

4.2.1. Model Description

The δ^{30}Si(OH)$_4$ of deep waters in the Canada Basin are the heaviest ever observed in the global ocean. To elucidate the mechanisms that control Si(OH)$_4$ concentrations and Si isotopic composition in the Arctic, we modified the PANDORA box model of *Broecker and Peng* [1986] to include the Arctic Ocean and to incorporate Si isotope fractionation by diatoms in a way similar to *Reynolds* [2009] (Figures 7a–7c). Water fluxes and

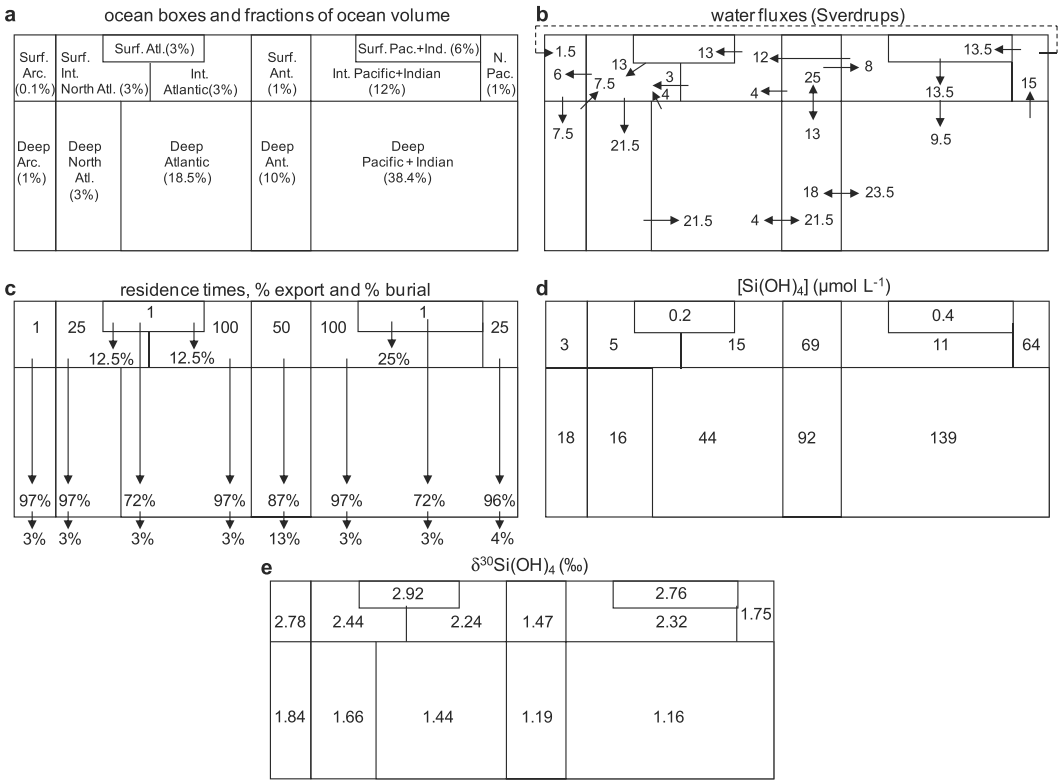

Figure 7. The PANDORA box model adapted from *Peng et al.* [1993], showing (a) box designations, with the percentage of the total ocean volume within each area shown in brackets (Surf.: Surface, Int.: Intermediate, Arc.: Arctic, Atl.: Atlantic, Ant.: Antarctic, Pac.: Pacific and Ind.: Indian), (b) water fluxes in Sverdrups (10^6 m^3 s^{-1}) between boxes [*Peng et al.*, 1993; *Codispoti and Lowman*, 1973; *Codispoti and Owens,* 1975], (c) residence times of the ocean boxes (years), percentages of exported particles and percentages of burial, (d) modeled $Si(OH)_4$ concentrations, and (e) modeled $\delta^{30}Si(OH)_4$ values.

residence times for the eleven boxes in the original PANDORA model follow *Broecker and Peng* [1986], and we added water fluxes between the Arctic and the North Pacific and North Atlantic based on *Codispoti and Lowman* [1973] and *Codispoti and Owens* [1975] (Figures 7b and 7c). The residence time of Arctic surface waters was assumed to match that in the surface Atlantic and Pacific + Indian Oceans (Figure 7c).

Input of $Si(OH)_4$ from rivers in the model is balanced by burial of diatom SiO_2 at the seafloor (each flux = 6.2 Tmol a^{-1}) [*Tréguer and De la Rocha,* 2013]. River input into the ocean was allocated as follows: 5% to the Arctic Ocean, 46% to the Atlantic Ocean, and 49% to the Pacific Ocean [*Durr et al.,* 2011]. Silicon inputs from deep-sea hydrothermal vents were ignored as they are a relatively minor source of Si compared to rivers [*Tréguer and De la Rocha,* 2013]. For each annual time step, the SiO_2 production in each surface box is calculated from the residence time of water in each surface box (R) as $1/R \times$ (box volume) $\times$ [$Si(OH)_4$]. The model runs freely in that there is no restoring of surface [$Si(OH)_4$]. At each annual time step all surface SiO_2 production is exported vertically and dissolved as a function of depth as indicated in Figure 7c. Burial of diatom opal is 3% of annual surface production [*Tréguer and De la Rocha,* 2013] in most basins with larger burial, mainly in the Southern and Pacific Oceans (Figure 7c), to reflect present-day opal preservation patterns [*DeMaster,* 2002]. A key aspect of the modified model circulation is that exchange between the Arctic and adjacent oceans occurs at relatively shallow depths with no exchange of Atlantic or Pacific deep-water with the Arctic (Figure 7b). This mimics the $<$50 m depth of the Bering Strait in the Pacific and the shallow inflow from the Atlantic across the Norwegian Sea and over the Fram Strait, though outflows from the Arctic through the Fram Strait can reach 2600 m [*Skagseth et al.*, 2008].

Because our estimated fractionation factor for the section (assuming an open system) did not differ from that measured in diatom cultures, the model employed the average fractionation factor from diatom culture studies of $\alpha = 0.9989$ ($^{30}\varepsilon = -1.1‰$) [*De La Rocha et al.*, 1997]. Note that using the average $^{30}\varepsilon$ of $-0.98 \pm 0.5‰$ from *Sutton et al.* [2013] changes the model outputs for deep waters by less than the current measurement

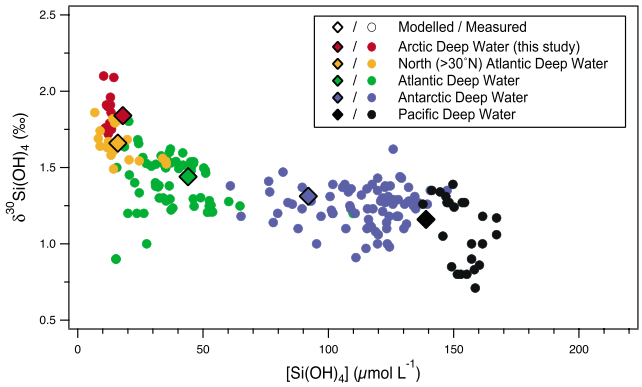

Figure 8. Comparison of measured deep-water (≥2000 m) $\delta^{30}Si(OH)_4$ (circles) with modeled $\delta^{30}Si(OH)_4$ (diamonds) as a function of $Si(OH)_4$ concentration for the deep-ocean basins defined in Figure 7a. Modeled values are from Figures 7d and 7e. Sources for measured deep-water values are as follows: this study (Arctic); *de Souza et al.* [2012a] and *Brzezinski and Jones* [2015] (North (>30°N) Atlantic); *De La Rocha et al.* [2000], *de Souza et al.* [2012a], and *Brzezinski and Jones* [2015] (Atlantic); *De La Rocha et al.* [2000], *Cardinal et al.* [2005], *Fripiat et al.* [2011a, 2011b], and *de Souza et al.* [2012b] (Antarctic); and *De La Rocha et al.* [2000], *Reynolds et al.* [2006], and *Beucher et al.* [2008] (Pacific).

error of 0.1‰. In the model, the $bSiO_2$ produced by diatoms is exported to depth and dissolves without fractionation as indicated in Figure 7c. Although *Demarest et al.* [2009] showed that fractionation occurs during opal dissolution, this variable was not included given the apparent complexities of Si isotope fractionation during this process, as discussed above (section 4.1.5).

The model was initiated by filling the simulated ocean with $Si(OH)_4$ at a uniform concentration of 71 μmol L^{-1} to reflect the world average concentration determined by *Tréguer and De la Rocha* [2013]. The initial $\delta^{30}Si(OH)_4$ was assigned a value of +0.85‰ everywhere based on $\delta^{30}Si$ measurements from rivers [*Georg et al.*, 2009]. River $\delta^{30}Si(OH)_4$ was held constant at +0.85‰. The model was run to equilibrium, requiring about 90,000 simulated years.

The water fluxes in the original PANDORA model were chosen to best match ^{14}C distributions [*Broecker and Peng*, 1986]. Our addition of the Arctic surface and deep boxes would alter simulated ^{14}C distributions, but we did not attempt to retune the model; rather, we relied on literature values to parameterize water fluxes between the Arctic and adjacent oceans. Two comparisons indicate this to be a reasonable approach. First, the model achieves mass balance with a whole ocean average $[Si(OH)_4]$ (75 μmol L^{-1}) and ocean residence time for Si of 16,000 years similar to the values of 71 μmol L^{-1} and 15,000 years obtained by *Tréguer et al.* [1995] using a version of PANDORA without the Arctic Ocean. Second, estimates of annual SiO_2 export from the modified PANDORA model compare well with the global analysis of *Dunne et al.* [2007] with agreement in estimated SiO_2 export among ocean regions being typically better than 30%; see supporting information Table S4.

4.2.2. Model Outputs

The model output is presented in Figures 7d and 7e. Silicic acid concentrations in intermediate and deep waters (Figure 7d) are all within 15% of the $[Si(OH)_4]$ values for the PANDORA model that *Nelson et al.* [1995] determined to best fit observations. The model also captures the main features of the global distribution of $\delta^{30}Si(OH)_4$ (Figure 7e), including the decrease in $\delta^{30}Si(OH)_4$ between the deep Atlantic and deep Pacific [*Reynolds,* 2009]. There is a relatively good match between the modeled deep-water $\delta^{30}Si(OH)_4$ and the in situ measurements for waters >2000 m deep, with the exception of the North Pacific where modeled isotope values are in the upper range of observations (Figure 8). Like the results of *Reynolds* [2009], strong ventilation in the North Atlantic leads to relatively low $[Si(OH)_4]$ concentrations and relatively heavy $\delta^{30}Si(OH)_4$ in the deep Atlantic (principally the North Atlantic) with exchange of heavy waters from the Arctic adding to this effect. Incomplete nutrient utilization in the Southern Ocean translates into relatively light $\delta^{30}Si(OH)_4$ in Southern Ocean deep water and heavy $\delta^{30}Si(OH)_4$ in intermediate and upper waters (Figure 8).

Most relevant to the current study is the model result that Arctic deep-waters have the most positive $\delta^{30}Si(OH)_4$ of all deep-ocean basins, with the modeled value of +1.84‰ being within the error of our average observed value of +1.88 ± 0.12‰ for waters >2000 m in CBDW (Table 3). In fact, the modeled deep Arctic value may be underestimated given that the chosen isotopic composition of rivers, +0.85‰, based on a global average, is lighter than values measured for large Arctic rivers during summer; +1.17 ± 0.13‰, +2.30 ± 0.09‰, +1.78 ± 0.14‰, and +1.36 ± 0.19‰ for the Lena, Yenissey, Ob, and Mackenzie rivers, respectively (B. C. Reynolds et al., unpublished, cited in *Pokrovsky et al.* [2013]). These heavier values were not used in the model as $\delta^{30}Si$ measured in rivers during summer can overestimate the discharge-weighted annual

average Si isotopic signature by up to 1‰ [*Pokrovsky et al.,* 2013]. Nevertheless, if the $\delta^{30}Si(OH)_4$ value for Arctic rivers in the model is increased to +1.5‰, the $\delta^{30}Si(OH)_4$ of the modeled deep Arctic Ocean increases from +1.84‰ to +1.92‰ leaving open the possibility that $Si(OH)_4$ from rivers contributes to the heavy isotopic composition of the deep Arctic.

The modeled surface Arctic water $\delta^{30}Si(OH)_4$ value, +2.78‰, is not the heaviest in the simulated surface ocean (Figure 7e), but it is a close match to the average value of +2.73 ± 0.08‰ for the underway surface samples (Table 2). The modeled North Atlantic intermediate/surface water $\delta^{30}Si(OH)_4$ value of +2.44‰ is comparable to the mean $\delta^{30}Si(OH)_4$ signature we calculated for the ATW water mass (+2.04 ± 0.11‰, Table 3).

The PANDORA model lacks the vertical resolution to reproduce the structure observed in our profiles, but major features are consistent with observations. The modeled North Pacific surface $\delta^{30}Si(OH)_4$ value (+1.75‰), the best proxy in the model for waters of Pacific origin in the UHL, is less positive than the modeled surface Arctic value (+2.78‰), and it is also less positive than the modeled intermediate/surface Atlantic water (+2.44‰), the best proxy for ATW. This is consistent with the minimum we observe in the $\delta^{30}Si(OH)_4$ vertical profiles between 100 and 200 m depth corresponding to Pacific-originated water in the UHL (Figure 3).

The model results support the hypothesis that heavy Si isotope values in the deep Arctic are caused by relatively shallow exchange with the Atlantic at intermediate depths, given that the latter introduces relatively nutrient-poor and isotopically heavy waters into the Arctic Ocean compared to that associated with the exchange of deep waters. That shallow exchange, coupled to further increases in $\delta^{30}Si(OH)_4$ from opal production and burial in Arctic waters, results in the deep Arctic Ocean having the heaviest $\delta^{30}Si(OH)_4$ signature in the simulated global ocean.

5. Conclusions

We present the first measurements of the seawater isotopic composition of Si in $Si(OH)_4$ and in $bSiO_2$ on the Beaufort shelf and in the Canada Basin. Values of $\delta^{30}Si(OH)_4$ were highest in surface waters, associated with biological fractionation during $Si(OH)_4$ uptake. We found a significant negative correlation between $\delta^{30}Si(OH)_4$ and the amount of Mackenzie River water present along the section, consistent with previous observations of low $\delta^{30}Si(OH)_4$ values in Mackenzie River water. Using an open system model, we estimated a biogenic Si isotope fractionation factor $^{30}\varepsilon$ of −0.97 ± 0.17‰ that agrees well with both laboratory and field estimates, suggesting that the apparent uniformity of $^{30}\varepsilon$ in the global ocean extends to the Arctic Ocean. However, the $\delta^{30}Si$ dynamics of our study region may be better represented by a closed system isotope model that yields lower values of $^{30}\varepsilon$, between −0.33‰ and −0.41‰, depending on how the contribution of sea-ice diatoms is incorporated. A significant positive correlation between $\delta^{30}Si\text{-}bSiO_2$ and sea-ice concentration leads us to believe that isotopically heavier sea-ice diatoms contributed to the isotopic composition of suspended $bSiO_2$ in surface waters. The distribution of Si isotopes was closely related to the distribution of water masses below the surface productive layer. Model results indicate that this is caused by the bathymetry that restricts exchange between the Arctic and adjacent oceans to relatively shallow depths. Exchange is dominated by the inflow into the Arctic of intermediate waters from the North Atlantic that carry low $[Si(OH)_4]$ and high $\delta^{30}Si(OH)_4$. Further $bSiO_2$ production and burial in Arctic waters drive $[Si(OH)_4]$ lower and $\delta^{30}Si(OH)_4$ higher with the result that the deep Canada Basin contains the isotopically heaviest $Si(OH)_4$ of all ocean basins.

Acknowledgments
We extend our appreciation to Maria Teresa Fernandez Sanchez and Arielle Kobryn for cruise preparations and logistic help during the research cruise, Jonathan Gagnon and Jean-Éric Tremblay for dissolved nutrient analysis, Jeffrey Krause for particulate SiO_2 analysis, and Katsumi Matsumoto, François Fripiat and another reviewer for critical comments on the manuscript. Thanks must also go to the CTD data acquisition group in ArcticNet for these basic but critical measurements and the calibration of the various probes. We also thank all scientists, officers, and crew members of the CCGS Amundsen who participated in the ArcticNet 0903 expedition. Funding for this project was provided by the Canadian IPY GEOTRACES program (D.E.V. and A.M., co-PIs). Most data presented graphically in this manuscript are shown in Tables 1 and 2 and in the supporting information section, whereas the rest of the data will be readily available by the corresponding author (D.E.V., dvarela@uvic.ca) upon request. All data is posted at the GEOTRACES Data Assembly Centre (GDAC; geotraces.dac@bodc.ac.uk).

References

Beucher, C. P., M. A. Brzezinski, and X. Crosta (2007), Silicic acid dynamics in the glacial sub-Antarctic: Implications for the silicic acid leakage hypothesis, *Global Biogeochem. Cycles*, *21*, GB3015, doi:10.1029/2006GB002746.

Beucher, C. P., M. A. Brzezinski, and J. L. Jones (2008), Sources and biological fractionation of silicon isotopes in the Eastern Equatorial Pacific, *Geochim. Cosmochim. Acta*, *72*, 3063–3073, doi:10.1016/j.gca.2008.04.021.

Beucher, C. P., M. A. Brzezinski, and J. L. Jones (2011), Mechanisms controlling silicon isotope distribution in the Eastern Equatorial Pacific, *Geochim. Cosmochim. Acta*, *75*, 4286–4294, doi:10.1016/j.gca.2011.05.024.

Broecker, W. S., and T. H. Peng (1986), Carbon cycle: 1985 glacial to interglacial changes in the operation of the global carbon cycle, *Radiocarbon*, *28*(2A), 309–327.

Brown, K. A., F. McLaughlin, P. D. Tortell, D. E. Varela, M. Yamamoto-Kawai, B. Hunt, and R. François (2014), Determination of particulate organic carbon sources to the surface mixed layer of the Canada Basin, Arctic Ocean, *J. Geophys. Res. Oceans*, *119*, 1084–1102, doi:10.1002/2013JC009197.

Brzezinski, M. A., and J. L. Jones (2015), Coupling of the distribution of silicon isotopes to the meridional overturning circulation of the north Atlantic ocean, *Deep Sea Res., Part II*, *116*, 79–88, doi:10.1016/j.dsr2.2014.11.015.
Brzezinski, M. A., and D. M. Nelson (1989), Seasonal changes in the silicon cycle within a Gulf Stream warm-core ring, *Deep Sea Res.*, *36*, 1009–1030, doi:10.1016/0198-0149(89)90075-7.
Brzezinski, M. A., J. L. Jones, K. D. Bidle, and F. Azam (2003), The balance between silica production and silica dissolution in the sea: Insights from Monterey Bay, California, applied to the global data set, *Limnol. Oceanogr.*, *48*, 1846–1854, doi:10.4319/lo.2003.48.5.1846.
Brzezinski, M. A., J. L. Jones, C. P. Beucher, and M. S. Demarest (2006), Automated determination of silicon isotope natural abundance by the acid decomposition of cesium hexafluosilicate, *Anal. Chem.*, *78*(17), 6109–6114, doi:10.1021/ac0606406.
Buckley, W. P., H. D. Scher, R. Thunell, M. A. Brzezinski, and T. D. Peterson (2010), Tracking changes in silicon isotopic composition during diatom descent and dissolution in the Cariaco Basin, American Geophysical Union, Fall Meeting 2010, abstract #PP11A-1429.
Cardinal, D., L. Y. Alleman, F. Dehairs, N. Savoye, T. W. Trull, and L. André (2005), Relevance of silicon isotopes to Si-nutrient utilization and Si-source assessment in Antarctic waters, *Global Biogeochem. Cycles*, *19*, GB2007, doi:10.1029/2004GB002364.
Cardinal, D., N. Savoye, T. W. Trull, F. Dehairs, E. E. Kopczynska, F. Fripiat, J.-L. Tison, and L. André (2007), Silicon isotopes in spring Southern Ocean diatoms: Large zonal changes despite homogeneity among size fractions, *Mar. Chem.*, *106*, 46–62, doi:10.1016/j.marchem.2006.04.006.
Carmack, E., and P. Wassmann (2006), Food webs and physical–biological coupling on pan-Arctic shelves: Unifying concepts and comprehensive perspectives, *Prog. Oceanogr.*, *71*(2), 446–477, doi:10.1016/j.pocean.2006.10.004.
Carmack, E. C., R. W. MacDonald, and J. E. Papadakis (1989), Water mass structure and boundaries in the Mackenzie Shelf estuary, *J. Geophys. Res.*, *94*(C12), 18,043–18,055, doi:10.1029/JC094iC12p18043.
Carmack, E. C., R. W. Macdonald, and S. Jasper (2004), Phytoplankton productivity on the Canadian Shelf of the Beaufort Sea, *Mar. Ecol. Prog. Ser.*, *277*, 37–50, doi:10.3354/meps277037.
Cavagna, A. J., F. Fripiat, F. Dehairs, D. Wolf-Gladrow, B. Cisewski, N. Savoye, L. André, and D. Cardinal (2011), Silicon uptake and supply during a Southern Ocean iron fertilization experiment (EIFEX) tracked by Si isotopes, *Limnol. Oceanogr.*, *56*(1), 147–160, doi:10.4319/lo.2011.56.1.0147.
Codispoti, L. A., and D. Lowman (1973), A reactive silicate budget for the Arctic Ocean, *Limnol. Oceanogr.*, *18*(3), 448–456, doi:10.4319/lo.1973.18.3.0448.
Codispoti, L. A., and T. G. Owens (1975), Nutrients transport through Lancaster Sound in relation to the Arctic Ocean's reactive silicate budget and the outflow of Bering Strait waters, *Limnol. Oceanogr.*, *20*(1), 115–119, doi:10.4319/lo.1975.20.1.0115.
De La Rocha, C. L., M. A. Brzezinski, and M. J. DeNiro (1996), Purification, recovery, and laser-driven fluorination of silicon from dissolved and particulate silica for the measurement of natural stable isotope abundances, *Anal. Chem.*, *68*(21), 3746–3750, doi:10.1021/ac960326j.
De La Rocha, C. L., M. A. Brzezinski, and M. J. DeNiro (1997), Fractionation of silicon isotopes by marine diatoms during biogenic silica formation, *Geochim. Cosmochim. Acta*, *61*(23), 5051–5056, doi:10.1016/S0016-7037(97)00300-1.
De La Rocha, C. L., M. A. Brzezinski, M. J. DeNiro, and A. Shemesh (1998), Silicon-isotope composition of diatoms as an indicator of past oceanic change, *Nature*, *395*, 680–683, doi:10.1038/27174.
De La Rocha, C. L., M. A. Brzezinski, and M. J. DeNiro (2000), A first look at the distribution of the stable isotopes of silicon in natural waters, *Geochim. Cosmochim. Acta*, *64*(14), 2467–2477, doi:10.1016/S0016-7037(00)00373-2.
De La Rocha, C. L., P. Bescont, A. Croguennoc, and E. Ponzevera (2011), The silicon isotopic composition of surface waters in the Atlantic and Indian sectors of the Southern Ocean, *Geochim. Cosmochim. Acta*, *75*(18), 5283–5295, doi:10.1016/j.gca.2011.06.028.
de Souza, G. F., B. C. Reynolds, J. Rickli, M. Frank, M. A. Saito, L. J. A. Gerringa, and B. Bourdon (2012a), Southern Ocean control of silicon stable isotope distribution in the deep Atlantic Ocean, *Global Biogeochem. Cycles*, *26*, GB2035, doi:10.1029/2011GB004141.
de Souza, G. F., B. C. Reynolds, G. C. Johnson, J. L. Bullister, and B. Bourdon (2012b), Silicon stable isotope distribution traces Southern Ocean export of Si to the eastern South Pacific thermocline, *Biogeosciences*, *9*(11), 4199–4213, doi:10.5194/bg-9-4199-2012.
de Souza, G. F., R. D. Slater, J. P. Dunne, and J. L. Sarmiento (2014), Deconvolving the controls on the deep ocean's silicon stable isotope distribution, *Earth Planet. Sci. Lett.*, *398*, 66–76, doi:10.1016/j.epsl.2014.04.040.
Demarest, M. S., M. A. Brzezinski, and C. P. Beucher (2009), Fractionation of silicon isotopes during biogenic silica dissolution, *Geochim. Cosmochim. Acta*, *73*(19), 5572–5583, doi:10.1016/j.gca.2009.06.019.
DeMaster, D. J. (1981), The supply and accumulation of silica in the marine environment, *Geochim. Cosmochim. Acta*, *45*(10), 1715–1732, doi:10.1016/0016-7037(81)90006-5.
DeMaster, D. J. (2002), The accumulation and cycling of biogenic silica in the Southern Ocean: Revisiting the marine silica budget, *Deep Sea Res., Part II*, *49*(16), 3155–3167, doi:10.1016/S0967-0645(02)00076-0.
Dunne, J. P., J. L. Sarmiento, and A. Gnanadesikan (2007), A synthesis of global particle export from the surface ocean and cycling through the ocean interior and on the seafloor, *Global Biogeochem. Cycles*, *21*, GB4006, doi:10.1029/2006GB002907.
Durr, H. H., M. Meybeck, J. Hartmann, G. G. Laruelle, and V. Ronbeix (2011), Global spatial distribution of natural riverine silica inputs to the coastal zone, *Biogeosciences*, *8*, 597–620, doi:10.5194/bg-8-597-2011.
Eakins, B. W., and G. F. Sharman (2010), *Volumes of the World's Oceans From ETOPO1*, NOAA Natl. Geophys. Data Cent., Boulder, Colo.
Ellwood, M. J., M. Wille, and W. Maher (2010), Glacial silicic acid concentrations in the Southern Ocean, *Science*, *330*(6007), 1088–1091, doi:10.1126/science.1194614.
Fernández-Méndez, M., C. Katlein, B. Rabe, M. Nicolaus, I. Peeken, K. Bakker, H. Flores, and A. Boetius (2015), Photosynthetic production in the central Arctic Ocean during the record sea-ice minimum in 2012, *Biogeosciences*, *12*(11), 3525–3549, doi:10.5194/bg-12-3525-2015.
Field, C. B., M. J. Behrenfeld, J. T. Randerson, and P. Falkowski (1998), Primary production of the biosphere: Integrating terrestrial and oceanic components, *Science*, *281*(5374), 237–240, doi:10.1126/science.281.5374.237.
Fripiat, F., D. Cardinal, J.-L. Tison, A. Worby, and L. André (2007), Diatom-induced silicon isotopic fractionation in Antarctic sea ice, *J. Geophys. Res.*, *112*, G02001, doi:10.1029/2006JG000244.
Fripiat, F., A. -J. Cavagna, F. Dehairs, S. Speich, L. André, and D. Cardinal (2011a), Silicon pool dynamics and biogenic silica export in the Southern Ocean inferred from Si-isotopes, *Ocean Sci.*, *7*(5), 533–547, doi:10.5194/os-7-533-2011.
Fripiat, F., A. -J. Cavagna, N. Savoye, F. Dehairs, L. André, and D. Cardinal (2011b), Isotopic constraints on the Si-biogeochemical cycle of the Antarctic Zone in the Kerguelen area (KEOPS), *Mar. Chem.*, *123*(1–4), 11–22, doi:10.1016/j.marchem.2010.08.005.
Fripiat, F., J. -L. Tison, L. André, D. Notz, and B. Delille (2013), Biogenic silica recycling in sea ice inferred from Si-isotopes: Constraints from Arctic winter first-year sea ice, *Biogeochemistry*, doi:10.1007/s10533-013-9911-8.
Georg, R. B., A. J. West, A. R. Basu, and A. N. Halliday (2009), Silicon fluxes and isotope composition of direct groundwater discharge into the Bay of Bengal and the effect on the global ocean silicon isotope budget, *Earth Planet. Sci. Lett.*, *283*, 67–74, doi:10.1016/j.epsl.2009.03.041.
Gosselin, M., M. Levasseur, P. A. Wheeler, R. A. Horner, and B. C. Booth (1997), New measurements of phytoplankton and ice algal production in the Arctic Ocean, *Deep Sea Res., Part II*, *44*(8), 1623–1644, doi:10.1016/S0967-0645(97)00054-4.

Grebmeier, J. M., L. W. Cooper, H. M. Feder, and B. I. Sirenko (2006), Ecosystem dynamics of the Pacific-influenced Northern Bering and Chukchi Seas in the Amerasian Arctic, *Prog. Oceanogr.*, *71*(2), 331–361, doi:10.1016/j.pocean.2006.10.001.

Hendry, K. R., and M. A. Brzezinski (2014), Using silicon isotopes to understand the role of the Southern Ocean in modern and ancient biogeochemistry and climate, *Quaternary Sci. Rev.*, *89*, 13–26, doi:10.1016/j.quascirev.2014.01.019.

Hendry, K. R., R. B. Georg, R. E. M. Rickaby, L. F. Robinson, and A. N. Halliday (2010), Deep ocean nutrients during the Last Glacial Maximum deduced from sponge silicon isotopic compositions, *Earth Planet. Sci. Lett.*, *292*(3–4), 290–300, doi:10.1016/j.epsl.2010.02.005.

Holzer, M., and M. A. Brzezinski (2015), Controls on the silicon isotope distribution in the ocean: New diagnostics from a data-constrained model, *Global Biogeochem. Cycles*, *29*, 267–287, doi:10.1002/2014GB004967.

Horn, M. G., C. P. Beucher, R. S. Robinson, and M. A. Brzezinski (2011), Southern Ocean nitrogen and silicon dynamics during the last deglaciation, *Earth Planet. Sci. Lett.*, doi:10.1016/j.epsl.2011.08.016.

Jones, E. P., and L. G. Anderson (1986), On the origin of the chemical properties of the Arctic Ocean halocline, *J. Geophys. Res.*, *91*, 10,759–10,767, doi:10.1029/JC091iC09p10759.

Karl, D. M., and G. Tien (1992), MAGIC: A sensitive and precise method for measuring dissolved phosphorus in aquatic environments, *Limnol. Oceanogr.*, *37*, 105–116, doi:10.4319/lo.1992.37.1.0105.

Lansard, B., A. Mucci, L. A. Miller, R. W. Macdonald, and Y. Gratton (2012), Seasonal variability of water mass distribution in the southeastern Beaufort Sea determined by total alkalinity and $\delta^{18}O$, *J. Geophys. Res.*, *117*, C03003, doi:10.1029/2011JC007299.

Macdonald, R. W., E. C. Carmack, F. A. McLaughlin, K. Iseki, D. M. Macdonald, and M. C. O'Brien (1989), Composition and modification of water masses in the Mackenzie Shelf estuary, *J. Geophys. Res.*, *94*(C12), 18,057–18,070, doi:10.1029/JC094iC12p18057.

Macdonald, R. W., E. C. Carmack, and D. W. R. Wallace (1993), Tritium and radiocarbon dating of Canada Basin deep waters, *Science*, *259*, 103–104, doi:10.1126/science.259.5091.103.

Macdonald, R. W., F. A. McLaughlin, and E. C. Carmack (2002), Freshwater and its sources during the SHEBA drift in the Canada Basin of the Arctic Ocean, *Deep Sea Res., Part I*, *49*(10), 1769–1785, doi:10.1016/S0967-0637(02)00097-3.

McClelland, J. W., R. M. Holmes, K. H. Dunton, and R. W. Macdonald (2012), The Arctic ocean estuary, *Estuaries Coasts*, *35*(2), 353–368, doi:10.1007/s12237-010-9357-3.

McLaughlin, F. A., E. C. Carmack, R. W. Macdonald, and J. K. Bishop (1996), Physical and geochemical properties across the Atlantic/Pacific water mass front in the southern Canadian Basin, *J. Geophys. Res.*, *101*, 1183–1197, doi:10.1029/95JC02634.

Nelson, D. M., P. Tréguer, M. A. Brzezinski, A. Leynaert, and B. Quéguiner (1995), Production and dissolution of biogenic silica in the ocean: Revised global estimates comparison with regional data and relationship to biogenic sedimentation, *Global Biogeochem. Cycles*, *9*, 359–372, doi:10.1029/95GB01070.

Peng, T. H., E. Maierreimer, and W. S. Broecker (1993), Distribution of ^{32}Si in the world ocean: Model compared to observation, *Global Biogeochem. Cycles*, *7*(2), 463–474, doi:10.1029/93GB00686.

Pichevin, L. E., B. C. Reynolds, R. S. Ganeshram, I. Cacho, L. Pena, K. Keefe, and R. M. Ellam (2009), Enhanced carbon pump inferred from relaxation of nutrient limitation in the glacial ocean, *Nature*, *459*, 1114–1117, doi:10.1038/nature08101.

Pokrovsky, O. S., B. C. Reynolds, A. S. Prokushkin, J. Schott, and J. Viers (2013), Silicon isotope variations in Central Siberian rivers during basalt weathering in permafrost-dominated larch forests, *Chem. Geol.*, *355*(C), 103–116, doi:10.1016/j.chemgeo.2013.07.016.

Ragueneau, O., and P. Tréguer (1994), Determination of biogenic silica in coastal waters: Applicability and limits of the alkaline digestion method, *Mar. Chem.*, *45*, 43–51, doi:10.1016/0304-4203(94)90090-6.

Reynolds, B. C. (2009), Modeling the modern marine $\delta^{30}Si$ distribution, *Global Biogeochem. Cycles*, *23*, GB2015, doi:10.1029/2008GB003266.

Reynolds, B. C., M. Frank, and A. N. Halliday (2006), Silicon isotope fractionation during nutrient utilization in the North Pacific, *Earth Planet. Sci. Lett.*, *244*, 431–443, doi:10.1016/j.epsl.2006.02.002.

Reynolds, B. C., et al. (2007), An inter-laboratory comparison of Si isotope reference materials, *J. Anal. Atom. Spectrom.*, *22*, 561–568, doi:10.1039/B616755A.

Riebesell, U., I. Schloss, and V. Smetacek (1991), Aggregation of algae released from melting sea ice: Implications for seeding and sedimentation, *Polar Biol.*, *11*(4), 239–248, doi:10.1007/BF00238457.

Simpson, K. G., J. É. Tremblay, Y. Gratton, and N. M. Price (2008), An annual study of inorganic and organic nitrogen and phosphorus and silicic acid in the southeastern Beaufort Sea, *J. Geophys. Res.*, *113*, C07016, doi:10.1029/2007JC004462.

Skagseth, Ø., T. Furevik, R. Ingvaldsen, H. Loeng, K. Mork, K. Orvik, and V. Ozhigin (2008), Volume and heat transports to the Arctic Ocean via the Norwegian and Barents Seas, in *Arctic–Subarctic Ocean Fluxes*, edited by R. Dickson, et al., pp. 45–64, Springer, Netherlands, doi:10.1007/978-1-4020-6774-7_3.

Sutton, J. N., D. E. Varela, M. A. Brzezinski, and C. P. Beucher (2013), Species-dependent silicon isotope fractionation by marine diatoms, *Geochim. Cosmochim. Acta*, *104*, 300–309, doi:10.1016/j.gca.2012.10.057.

Tréguer, P., and C. L. De La Rocha (2013), The world ocean silica cycle, *Annu. Rev. Mar. Sci.*, *5*, 477–501, doi:10.1146/annurev-marine-121211-172346.

Tréguer, P. J., D. M. Nelson, A. J. Van Bennekom, D. J. DeMaster, A. Leynaert, and B. Quéguiner (1995), The silica balance in the world ocean: A reestimate, *Science*, *268*(5209), 375–379, doi:10.1126/science.268.5209.375.

Tremblay, J.-É., K. Simpson, J. Martin, L. Miller, Y. Gratton, D. Barber, and N. M. Price (2008), Vertical stability and the annual dynamics of nutrients and chlorophyll fluorescence in the coastal, southeast Beaufort Sea, *J. Geophys. Res.*, *113*, C07S90, doi:10.1029/2007JC004547.

Tremblay, J. É., D. Robert, D. E. Varela, C. Lovejoy, G. Darnis, R. J. Nelson, and A. R. Sastri (2012), Current state and changing trends in Canadian Arctic marine ecosystems: I. Primary production, *Clim. Change*, *115*, 161–178, doi:10.1007/s10584-012-0496-3.

Varela, D. E., C. J. Pride, and M. A. Brzezinski (2004), Biological fractionation of silicon isotopes in Southern Ocean surface waters, *Global Biogeochem. Cycles*, *18*, GB1047, doi:10.1029/2003GB002140.

Varela, D. E., D. W. Crawford, I. A. Wrohan, S. N. Wyatt, and E. C. Carmack (2013), Pelagic primary productivity and upper ocean nutrient dynamics across Subarctic and Arctic Seas, *J. Geophys. Res. Oceans*, *118*, 7132–7152, doi:10.1002/2013JC009211.

Whitledge, T. E., S. Malloy, C. J. Patton, and C. D. Wirick (1981), Automated nutrient analysis in seawater, *Tech. Rep. BNL 51398*, Brookhaven National Lab., Upton, New York, doi:10.2172/5433901.

Wille, M., J. Sutton, M. J. Ellwood, M. Sambridge, W. Maher, S. Eggins, and M. Kelly (2010), Silicon isotopic fractionation in marine sponges: A new model for understanding silicon isotopic variations in sponges, *Earth Planet. Sci. Lett.*, *292*(3–4), 281–289, doi:10.1016/j.epsl.2010.01.036.

Wyatt, S. N., D. W. Crawford, I. A. Wrohan, and D. E. Varela (2013), Distribution and composition of suspended biogenic particles in surface waters across Subarctic and Arctic Seas, *J. Geophys. Res. Oceans*, *118*, 6867–6880, doi:10.1002/2013JC009214.